Title: An endogenous scaling mechanism in zebrafish appendages that controls two-pore potassium-leak channel activity to regulate morphogen and growth factor transcription.

Chao Yi[1,2], Tim WGM Spitters[1*], Ezz Al-Din Ahmed Al-Far[3*], Sen Wang[1,2], Simian Cai[1], Xin Yan[1], Kaomei Guan[3], Michael Wagner[3,4], Ali El-Armouche[3] and Christopher L. Antos[1,3]†

[1]School of Life Sciences and Technology, ShanghaiTech University, 230 Haike Road, Shanghai, People's Republic of China.

[2] CAS Center for Excellence in Molecular Cell Science, Shanghai Institute of Biochemistry and Cell Biology, Chinese Academy of Sciences, University of Chinese Academy of Sciences

[3]Institut für Pharmakologie und Toxikologie, Technische Universität Dresden, Fetscherstraße 74, 01307 Dresden, Germany

[4]Abteilung für Rhythmologie, Herzzentrum Dresden, Technische Universität Dresden, Fetscherstraße 76, 01307 Dresden, Germany

*These two authors contributed equally.

Running Title: Kcnk5b coordination of developmental transcription

Key words: regeneration, development, zebrafish appendages, proportional growth, membrane potential, morphogens

†Corresponding Author:
Christopher L. Antos
School of Life Sciences and Technology
ShanghaiTech University,
230 Haike Road
Pudong, New District,
Shanghai, China 201210
clantos@shanghaitech.edu.cn
christopher.antos@tu-dresden.de

Abstract

The increase in activity of the two-pore potassium-leak channel Kcnk5b maintains allometric juvenile growth of adult zebrafish appendages. However, it remains unknown how this channel maintains allometric growth and how its bioelectric activity is regulated to scale these anatomical structures. We show the activation of Kcnk5b is sufficient to activate several development programs, including two morphogen pathways involved in tissue formation, *shh* and *wnt* signaling. We provide in vivo transplantation evidence that the activation of developmental programs is cell autonomous and Kcnk5b can induce the expression of these developmental programs in cultured mammalian cell lines. We also demonstrate how post-translational modification of serine 345 in Kcnk5b by calcineurin regulates channel activity and controls these developmental programs to scale the fin. Thus, we show how an endogenous bioelectric program is regulated and promotes coordinated developmental signaling to generate and scale a vertebrate appendage.

Introduction

Tissue scaling involves the coordinated control of developmental programs, since anatomical structures consist of different tissues that form in a coordinated manner and grow proportionally with each other and with the body. While there are several developmental signals known to regulate cell proliferation and tissue formation, mechanisms that concomitantly activate several developmental signals to synchronize the growth of multi-tissue appendages and organs in a manner that is coordinated with body proportions remain poorly defined.

There is growing evidence that several biological phenomena involved in tissue generation and growth are influenced by electrophysiological changes in "non-excitable" cells (Sundelacruz et al., 2009). Several cell behaviors are affected by the addition of electric currents (McCaig et al., 2005): cell migration, cell proliferation, cell differentiation, gene transcription and consequently tissue formation are all altered by the application of an exogenous current (Baer and Colello, 2016; Bartel et al., 1989; Blackiston et al., 2009; Borgens et al., 1977; Geremia et al., 2007; Sundelacruz et al., 2009; Yasuda, 1974; Zhao et al., 2002). The culmination of these findings have led to the hypothesis that bioelectrical fields exist that have higher order organizational non-cell-autonomous properties in the developmental of anatomical structures [For review, see (Levin, 2014; Messerli and Graham, 2011)].

As a regulator of membrane potential, K^+ conductance is an important component of the electrophysiological properties of cells. Evidence that illustrates the importance of K^+ conductance in tissue formation comes from studies in which disruption of inward rectifying K^+ channels of the Kir2 family can cause cranial facial defects, abnormal number of digits and reduced digit size (Andersen et al., 1971; Canun et al., 1999; Sansone et al., 1997; Tawil et al., 1994; Yoon et al., 2006a; Yoon et al., 2006b; Zaritsky et al., 2000). A striking finding concerning the coordinated control of cell behavior is the formation of eye structures by overexpressing different ion channels that alter membrane potential in early *Xenopus* embryos (Pai et al., 2012): overexpression and activation of a glycine-gated chloride channel in cells that form the eye interferes with eye formation, while overexpression of a dominant-negative K^+-ATP channel simulates ectopic eye formation even in unexpected locations on the body (Pai et al., 2012). These findings illustrate that changes in the membrane potential of cells can have significant impacts on the development of anatomical structures. However, how

electrophysiological information associates with the multiple necessary signals that control formation and/or growth of multi-tissue structures remains unclear.

The development of body structures not only involves forming tissues, it also involves coordinating the growth of each contributing tissue cell. To form organs that correctly scale with the body, each tissue grows either isometrically (grows with the same rate as the body) or allometrically (disproportionally grows in relation to the growth of the body). The zebrafish mutants *another long fin* (*alf*), *long fin* (*lof*) and *schleier* (*schl*) display continued allometric growth of each appendage from the juvenile stage into the adult stage (Lanni et al., 2019; Perathoner et al., 2014; Stewart et al., 2020). The dominant allometric growth phenotype of *alf* is due to mutations in the transmembrane pore region of *kcnk5b* (Perathoner et al., 2014), encoding a two-pore K^+-leak channel that regulates membrane potential by outward flow of K^+ from the cell (Goldstein et al., 2001). The dominant phenotype of *lof* is linked to elevated expression of a voltage-gated potassium channel *Kcnh2a* (Stewart et al., 2020). The phenotype of *schl* is due to dominant-negative mutations in *scc4* (Lanni et al., 2019), encoding a K^+-Cl^- cotransporter that regulates intracellular K^+ levels in a chloride-dependent manner (Marcoux et al., 2017). *alf*, *lof* and *schl* demonstrate the importance of K^+ conductance and ultimately of electrophysiological signals for the correct body-to-appendage proportions. Despite the connection between K^+ conductance and the proportional growth of the fins, it remains unclear how K^+-mediated signal translates into coordinated growth of the fish appendage and how any K^+ channel is regulated to scale tissue.

We show that activity of the single two-pore K^+-leak channel Kcnk5b is sufficient to induce the activation of two important morphogen pathways (Shh and β-catenin-dependent Wnt) not only in the adult fin but also in the larva. Our data also indicates that this induction is cell autonomous, indicating that increases in membrane potential caused by Kcnk5b regulate growth through the regulation of these developmental pathways. Furthermore, we show that Kcnk5b has similar inductive effects in mammalian cells and that this phenomenon can be induced by other two-pore Kcnk channels, supporting the conclusion that the developmental programs are regulated by the same electrophysiological change induced by potassium leak. Lastly, we show how post-translational modification of Kcnk5b at Serine345 by calcineurin regulates its electrophysiological activity and consequently the scaling of zebrafish fins. Thus, we describe an endogenous cell-autonomous mechanism through which electrophysiological signals induce and coordinate morphogen and growth factor signals to mediate the scaling of an anatomical structure.

Results

Kcnk5b is sufficient to induce several developmental gene programs in different cell types in adult and larva.

Mutations in the two-pore K^+-leak channel Kcnk5b that increase its activity lead to enhanced growth of the zebrafish appendages (Perathoner et al., 2014). While this finding implicates the importance of bioelectric signaling in appendage scaling, it remains unknown how the activity of a single K^+ channel is integrated with the developmental controls that generate new appendage tissues. Growth of any appendage involves the coordinated activation of specific morphogen and growth factor pathways: Shh, β-catenin-dependent Wnt, Bmp, Fgf and Retinoic acid. Therefore, to begin to determine how this channel is involved in the coordinated growth of the entire fin, we generated transgenic zebrafish that expresses *kcnk5b* under the control of conditionally inducible promoter (heat-shock promoter) to temporally activate this channel in adult fins. After a single ten-minute heat-shock pulse of the Tg[*hsp70*:*kcnk5b*-GFP] transgene, we observed significant activation of *shh* and *lef1* (β-catenin-dependent Wnt) (Fig. 1Aa), as well as an increase in *aldh1a2* (retinoic acid) and *msxb* (Bmp) (Fig. 1Ab) within 6 hours by qRT-PCR. The elevated expression of *shh* and *lef1* continued 12 hours after the single pulse (Fig. 1Ba), while the other genes returned to control values or were down regulated (Fig. 1Bb). The transgenic expression of the channel emerged as a lattice pattern indicating that Kcnk5b-GFP was localized on cell membranes (Suppl. Fig. 1A-C). The induction of these developmental genes is linked to *kcnk5b* expression, since their up-regulation coincided with the temporal expression of the *kcnk5b*-GFP transgene (Suppl. Fig. 1D,E), and all genes were down-regulated by 24 hours after the single heat-shock pulse (Suppl. Fig. 1F). When we maintained chronic expression of the transgene by heat shocking the caudal fin for 10 minutes once per day for 3 days, we observed expression of *lef1*, *shh*, *aldh1a2* as well as *pea3* over controls (Fig. 1C). Together, these data show that Kcnk5b is sufficient to induce certain developmental programs as though it were a part of a signaling mechanism for tissue generation.

To examine the spatial expression of the two genes most responsive to Kcnk5b, we performed in situ hybridization experiments for *shh* and *lef1*. We observed the localization of *shh* and *lef1* in the distal tip of the fin (Fig. 1Da-d) were growth normally occurs, and cross sections through the fins showed that these genes are expressed in overlapping patterns in the epidermal/dermal tissues (Fig. 1Ea-d). We also assessed increases in Shh and Lef1 protein levels after the heat-shock induction of *kcnk5b*-GFP (Fig. 1F,G). Because Lef1 conveys β-catenin-dependent Wnt signaling by acting as transcriptional platform for β-catenin, we

examined protein expression of β-catenin and observed no significant differences in its overall levels (Fig. 1F,G). However, when we examined β-catenin protein distribution in the fin tissues by immunohistochemistry staining, we observed an increased number of nuclei with β-catenin co-staining in the dermal and mesenchyme tissues of the fin (Fig. 1H,I) despite no significant differences in the measured β-catenin-associated fluorescence intensities (Fig. 1J). Together, these results indicate that increased expression of *kcnk5b* is sufficient to activate the developmental signaling programs involved in generation of new tissue. They also suggest a direct relationship between K^+ conductance and the transcriptional regulation of at least two important morphogen pathways.

To test whether increasing the activity of Kcnk5b has the same transcriptional effect on these developmental pathways in another *in vivo* context, we induced the expression of *kcnk5b* in the zebrafish larva. We observed that *lef1* and *shh* expression increased, while the other genes representing the other pathways did not (Fig. 2A). We confirmed the increase in β-catenin-dependent Wnt signaling by crossing the heat-shock-inducible transgenic Tg[*hsp70*:*knck5b*-GFP] line with the β-catenin-dependent Wnt transgenic reporter line Tg[*7xTCFsamois*:mCherry]. While the double-transgenic fish Tg[*hsp70*:*kcnk5b*-GFP; *7xTCFsamois*:mCherry] displayed limited expression of mCherry before heat-shock induction of the *kcnk5b*-GFP transgene (Fig. 2Ba,b,g), after heat shock, double-transgenic fish showed a broad increase in reporter mCherry expression (Fig. 2Bd,e,g). From histological cross sections of double-transgenic larva, we observed that mCherry was upregulated broadly in the body of the animal (Fig. 2C). Furthermore, we observe an increase in the proportional growth of the dorsal-to-ventral dimensions of the caudal finfold form induction of *kcnk5b*-GFP by one daily 10-minute pulse for 3 days (Fig. 2D), showing a functional effect on growth by Kcnk5b. Together, these results indicate that the increased Kcnk5b activity is sufficient to promote *shh* and β-catenin-dependent Wnt signaling in several different tissue types.

Activation of β-catenin-dependent Wnt reporter by Kcnk5b is cell autonomous in several different tissues

Previous work implicates bioelectric intercellular communication as a mechanism for how bioelectricity can influence tissue growth (McLaughlin and Levin, 2018), and changes in K^+ channel activity have been shown to regulate different cell behaviors in a non-cell-autonomous manner (Morokuma et al., 2008; Pai et al., 2015). The broad activation of the β-catenin-dependent Wnt reporter in several tissues (Fig. 2) and Kcnk5b's ability to scale all the

tissues of the fin appendages suggest that Kcnk5b acts via non-cell autonomous communication among cells. To determine whether the observed Kcnk5b-mediated induction of gene expression is due to intercellular communication (e.g., through extracellular ligands such as Wnt) or due to cell autonomous activation of transcription, we transplanted cells from Tg[*hsp70*:*kcnk5b*-GFP; 7xTCF*samois*:mCherry] transgenic embryos into embryos harboring only the Tg[7xTCF*samois*:mCherry] transgene and then raised mosaic embryos as larva (Fig. 3A). Analyses of the mosaic larva showed the reported developmental expression of the β-catenin-dependent Wnt reporter before heat shock (Fig. 3Ba,e,i,m)(Moro et al., 2012). However, after heat-shock induction of the Tg[*hsp70*:*kcnk5b*-GFP] transgene (Fig. 3Bb,f,j,n), we observed ectopic activation of 7xTCF*samois*:mCherry reporter in all chimeric embryos. GFP-mCherry-positive cells appeared in tissues in the head (Fig. 3Bb,c,d), in skeleton surrounding the eye (Fig. 3Bf,g,h), in trunk muscles (Fig. 3Bj,k,l) and in skin (Fig. 3Bn,o,p). From closer inspection, we observed co-expression in neurons in the head (Fig. 3Ca-c), in the ectodermal bones of the skull (Fig. 3Cd-f), mandible bone and cartilage (Fig. 3Cg-i), mesenchyme surrounding the otic vesicle (Fig. 3Cj-l), epithelial cells in the finfold (Fig 3Co-r) and individual striated muscle cells of the trunk (Fig. 3Cr-t). We counted the number of GFP and mCherry positive cells in the different tissues and observed that all Kcnk5b-GFP-positive cells were mCherry positive (Fig. 3C). Moreover, in all tissues, the ectopic mCherry expression was always limited to the Kcnk5b-positive cells (Fig. 3B-D). Together, these data support two conclusions: one, the activation of the β-catenin-dependent reporter by Kcnk5b is cell autonomous; and two, Kcnk5b is able to promote the expression of the Wnt reporter in diverse tissue types.

As a K^+-leak channel, Kcnk5b's activity should decreases intracellular K^+ levels. We performed Fluorescence Lifetime Microscopy (FLIM) analysis with an established genetic sensor for K+ to measure intracellular K^+ levels (Shen et al., 2019). This sensor uses the FRET potential between two fluorophores that are joined by a K^+-binding linker. Changes in FRET due to K^+ binding results in changes in the fluorescence lifetime of the fluorophores, which allows for the assessment of intracellular K^+ levels. Transfection of the channel in Human Embryonic Kidney HEK293T cells (Suppl. Fig. 3A-L) resulted in significant increase in CFP fluorescence lifetime due to decreased FRET of the sensor compared to control transfected cells (Fig. 4Aa-c,g), which indicated reduced intracellular K^+ levels in the cells that express Kcnk5b (Fig. 4Ad-g). Additional higher resolution assessments along the lateral borders of cells showed similar increases in CFP fluorescence lifetime along the plasma

membrane, indicating expected reduction of K^+ levels at the cell membrane by active Kcnk5b (Suppl. Fig. 3M-O).

To test whether activity *kcnk5b* promotes the gene expression profile in mammalian cells that we observed in the zebrafish, we established stable HEK293T (HEK) cells lines that either express GFP or zebrafish *kcnk5b*-GFP. From qRT-PCR analyses comparing HEK cells expressing either GFP or *kcnk5b*-GFP, we observed an increase in SHH and PEA3 expression (Fig. 4Ba) and the down-regulation of LEF1, ALDH1a2 and MSX1 (Fig. 4Bb). To determine whether this transcriptional response is specific to Kcnk5b or is a general response to two-pore K^+-leak channels, we transfected cells with one of two K^+-leak channels Kcnk9 and Kcnk10 (Suppl. Fig 4A,B). Transfection of HEK cells with these two other channels resulted in the same transcriptional profile as Kcnk5b (Fig. 4C), indicating that the transcriptional response to Kcnk5b is a response to the electrophysiological changes associated with intracellular K^+ leak.

The difference between the transcriptional responses of the zebrafish adult, larva and HEK cells indicates that different cell types will have different responses to Kcnk5b electrophysiological activity. Therefore, we examined the transcriptional responses to Kcnk5b in other mammalian cell lines. In HeLa cells, Kcnk5b induced PEA3 and LEF (Fig. 4D). From the N2A (neural carcinoma) cell line, we observed the increase of ALDH1a2 (Fig. 4E) but decreases in SHH, LEF1 and PEA3 (Fig. 4F). In the MYF7 epithelial carcinoma cell line, Kcnk5b induced ALDH1a2, PEA3 and MSX1 (Fig. 4G) We propose that the variability in genes that are transcribed may explain why the solitary change in the activity of this channel in all cells of the fin leads to the variable transcriptional responses needed to promote coordinated growth of a multi-tissue anatomical structure. These results also reveal that Kcnk channel activity is sufficient to induce the transcription of different developmental pathways in different mammalian cells types and that K^+ conductance-mediated induction of developmental transcription is shared among vertebrate species.

Calcineurin regulates Kcnk5b channel activity and Kcnk5b-mediated gene transcription

We previously showed that the phosphatase calcineurin acts as a molecular switch between isometric and allometric proportional growth of the zebrafish fins (Kujawski et al., 2014). The similarities in the phenotypes produced by calcineurin inhibition and by the mutations in Knck5b that enhance Kcnk5b channel activity suggest a direct functional

241 relationship between them (Kujawski et al., 2014; Perathoner et al., 2014). Based on whole-
242 cell patch-clamp experiments, the mutations in *kcnk5b* that maintain allometric growth of the
243 fins also increased K^+ conductance at the plasma membrane (Perathoner et al., 2014).
244 Therefore, we hypothesized that calcineurin inhibition will increase *in vivo* K^+ conductance
245 and promote allometric growth of the zebrafish fins (Fig. 5A). To test whether calcineurin
246 alters the channel activity of Kcnk5b, we examined whether the activity of Kcnk5b is altered
247 by calcineurin. Comparison of whole-cell patch-clamp measurements using HEK cells
248 showed that Kcnk5b expression increases current density due to K^+ leak from the cells (Fig.
249 5B), as we observed from FRET-FLIM intracellular K^+ measurements (Fig. 4A). However,
250 cells co-expressing both *knck5b* and calcineurin decreased the K^+ conductance of the cells
251 compared to cells expressing *kcnk5b* alone (Fig. 5B). We then tested whether inhibition of the
252 endogenous calcineurin activity in the HEK cells by the calcineurin inhibitor FK506 affects
253 Kcnk5b channel activity. We found that FK506 treatment of cells expressing *kcnk5b* resulted
254 in a significant increase in K^+ current compared with DMSO-treated *kcnk5b*-expressing cells
255 (Fig. 5C). These results show that changes in calcineurin activity alter Kcnk5b channel
256 activity in a manner that is constant with the enhanced fin growth induced by calcineurin
257 inhibition and the increased channel activity of the *kcnk5b* zebrafish mutants, which indicates
258 a functional interaction between calcineurin and Kcnk5b.

259 Calcineurin interacts with its substrates at particular amino acid sequence sites (Grigoriu
260 et al., 2013). Our analysis of the amino acid sequence in the C-terminal cytoplasmic tail of
261 Kcnk5b suggests a functional calcineurin binding site (LVIP) is present (Fig. 5A, red letters).
262 To test for functional interaction at this site, we mutated the amino acid sequence (Fig. 5D,
263 red letters) and assessed how the mutation affected the ability of calcineurin to regulate the
264 channel. Compared to the decrease in activity of the wild-type channel after co-transfection
265 with calcineurin, co-transfection of the Kcnk5b mutant lacking the calcineurin binding site
266 with calcineurin (Kcnk5bmut+CaN) showed that the mutation made the channel resistant to
267 calcineurin-mediated inhibition (Fig. 5D). The resistance of the Kcnk5bmut to calcineurin
268 indicated that the repression of channel activity on Kcnk5b by calcineurin is due to the
269 interaction of these to proteins at the LVIP site.

270 The regulation of Kcnk5b by calcineurin suggests that changes in calcineurin activity
271 will have an effect on the Kcnk5b-dependent gene expression. To assess whether the
272 activation of SHH by Knck5b can be altered by calcineurin, we compared the expression of
273 SHH between HEK cells stably expressing GFP and HEK cells stably expressing the Kcnk5b
274 channel as well as between HEK cells stably expressing the channel after transfection with

calcineurin. We observed that compared to channel expression alone, co-expression of calcineurin decreased the Kcnk5b-mediated induction of SHH (Fig. 5E) and PEA3 (Fig. 5F). To determine whether calcineurin effect on Kcnk5b-medidated SHH expression is specific to Kcnk5b, we transfected HEK cells with Kcnk9 or Kcnk10. Both Kcnk9 and Kcnk10 lack identifiable calcineurin binding sites (Suppl. Fig. 4A,B), and we observed that unlike the effect on Kcnk5b, calcineurin had no effect on the induction of SHH (Fig. 5G) or PEA3 (Fig. 5H) by Kcnk9 or by Kcnk10, indicating that calcineurin's regulation of the electrophysiological induction of SHH and PEA3 transcription is specific to Kcnk5b.

Calcineurin regulates Kcnk5b through S345 to scale the fin

As a phosphatase, calcineurin should regulate Kcnk5b by dephosphorylating the channel at specific serine or threonine residues. A specific serine in the C-terminal tail represented a typical consensus serine-proline (Ser345-Pro346) phosphorylation site for calcineurin (Fig. 6A). Therefore, we hypothesized that calcineurin inhibits the activity the Kcnk5b channel by dephosphorylating this serine. We tested whether rendering the Kcnk5b channel unphosphorylatable at this serine by alanine substitution (S345A) would decrease the channel's activity. Whole-cell patch-clamp experiments of the *kcnk5bS345A* showed a significant decrease in K^+ conductance of the channel compared to the wild-type (*kcnk5bS345*) control (Fig. 6B). To assess the specificity of the reduction effect for this serine, we also systematically substituted adjacent serines with alanines and subsequently measured channel activity (Suppl. Fig. 5A). While *kcnk5bS345A* showed reduction in activity, the substitution of other serines did not (Fig. 6C, Suppl. Fig. 5A-D).

To determine whether the activity of the Kcnk5b channel is associated with the phosphorylation state of this serine, we exchanged the serine for a glutamic acid to mimic serine phosphorylation (*kcnk5bS345E*) (Fig. 6C). Expression of this mutant displayed elevated K^+ conductance compared to *knck5bS345* wildtype channel (Fig. 6D). Moreover, the *kcnk5bS345E* mutant was resistant to calcineurin-mediated inhibition (Fig. 6D), while substitution of other serines with glutamic acid not only had no effect on channel activity, calcineurin could still regulated the channel (Suppl. Fig. 5A,E,F). Together, these results indicate that S345 is the important post-translational regulatory serine involved in calcineurin-mediated regulation of Kcnk5b activity.

To determine whether there is a functional relationship between fin scaling and S345-mediated Kcnk5b channel activity, we placed the cDNA of each channel version (wild-type *kcnk5bS345*, *kcnk5bS345E* or *kcnk5bS345A*) under the control of the heat-shock inducible

hsp70 promoter to generate conditionally inducible transgenes for *in vivo* expression in the fish. We induced the expression of each transgene by heat shocking the caudal fins once daily and subsequently measured the length of the fin in relation to the length of the body (fin-to-body ratio). After 12 days of the heat-shock regimen, we noticed differences between the rates of the regenerating caudal fins lobes of the different transgenic lines (Fig. 6E) after standardizing the length of each fin to the length of the body (Suppl. Fig. 5G). By assessing regenerating lobe-to-body measurements over time, we observed that Tg[*hsp70*:*kcnk5bS345E*] fish maintained the highest rates of allometric regenerative growth, while Tg[*hsp70*:*kcnk5bS345A*] displayed the lowest growth rates of the transgenic lines (Fig. 6E). There was no significant change in the rates of growth of the bodies (Suppl. Fig. 5G). We also assess the final proportional size of unamputated fin lobes between the different transgenic lines, and we observed a linear relationship between the proportional length of the unamputated lobes and the phosphorylation status of the channels: the S345A dephosphorylation mimic displayed the smallest growth proportions (Fig. 6I), the S345E phosphorylation mimic displayed the largest growth proportions (Fig. 6I), and the average value of the wild-type regulatable version of the channel was between the highly active S345E and marginally active S345A mutants (Fig. 6I). In addition to allometric growth, the genomic *kcnk5b* mutant *another long fin* (*alf*) also displays disruption of the normal bone segmentation pattern (Perathoner et al., 2014). To determine the extent that the different serine mutants phenocopy the segmentation defect of *alf*, we measured each bone segment from the base to the distal tip of the fin of the regenerating lobes heat-shocked fish, and we observed that the extent of segmentation defects was directly related to the activity of the channel: overexpression of *kcnk5bS345E* displayed a greater increase in segment length than overexpression of *kcnk5bS345A* (Fig. 6J). These results directly link post-translational regulation of channel activity with the degree of allometric growth and bone segmentation of the fin. Our ability to control the rate of growth and bone segmentation by mimicking a specific post-translational modification that can be mediated by calcineurin and that correspondingly determines the level of Kcnk5b activity supports the conclusion that calcineurin regulation of Kcnk5b is an *in vivo* electrophysiological mechanism through which controlling the potassium conductance of cells scales a vertebrate appendage.

Discussion

Anatomical structures consist of a combination of different tissue types that develop and grow in a coordinated manner. Recent discoveries show that K^+ channels regulate the scaling of fish appendages, but it is still unclear how this electrophysiological signal controls several diverse developmental phenomena within this anatomical structure to achieve coordinated developmental growth. Our results reveal that this *in vivo* electrical signal to induce multiple important developmental programs, namely Shh and Lef1-mediated Wnt signaling, in the fish fins and larva to scale a vertebrate appendage.

Two-pore K^+-leak channels such as Kcnk5b allow K^+ to cross the membrane to establish an electrochemical equilibrium, this activity directly affects the membrane potential of the cell (Goldstein et al., 2001). Normally, the concentration of K^+ is higher on the cytoplasmic side of the plasma membrane due to continual active transport of K^+ into the cell by the ATP-dependent Na^+/K^+ pumps (Shattock et al., 2015). As a leak channel, opening of Kcnk5b causes a flow of K^+ out of the cell, which hyperpolarizes the membrane potential (Goldstein et al., 2001). The finding that mutations that increase Kcnk5b channel activity maintaining allometric growth (Perathoner et al., 2014) argue that such changes in membrane potential promote disproportional growth. Our findings that conditional induction of Kcnk channel activity is sufficient to induce morphogen pathways (Fig. 1,2,4) in different *in vivo* and *in vitro* contexts furthers these original findings by demonstrating transcriptional control of developmental programs by different two-pore K^+-leak channels.

In addition to K^+-leak channels, cells regulate intracellular K^+ through different channels and exchangers. Inward rectifying K^+ channels allow K^+ to enter the cell along the ion's electrochemical gradient. Exchangers will exchange K^+ with different substrates (e.g., Na^+) to facilitate the entry or removal of K^+ based on the concentration gradient of K^+ and the exchanged substrate. Previous findings show the importance of the inward rectifying K^+ channel Kir2 for cranial-facial and digit defects in humans (Andersen et al., 1971; Canun et al., 1999; Sansone et al., 1997; Tawil et al., 1994; Yoon et al., 2006a; Yoon et al., 2006b). Knockout of the mouse Kir2 channels results in similar head and digit defects (Zaritsky et al., 2000), and dominant-negative inhibition of the Drosophila Kir2 leads to wing appendage defects that are analogous to the human and mouse appendage defects (Dahal et al., 2012). While the mammalian phenotypes remain unexplained, the defects in the Drosophila wings have been linked to reduced Dpp (BMP) signaling (Dahal et al., 2012), suggesting that intracellular K^+ homeostasis is important for BMP signaling.

Removal of an ATP-sensitive K^+ channel in the early *Xenopus* embryo disrupts eye formation, while ectopic expression of this channel will produce ectopic eyes in the head and in locations that were not considered to be competent for producing eyes (Pai et al., 2012). The ability to ectopically generate eyes was linked to electrophysiological hyperpolarization of the cells and the activation of Pax6-eyeless gene (Pai et al., 2012), a master regulator for eye development (Chow et al., 1999; Halder et al., 1995). In planaria, shortly after wounding, membrane depolarization acts as an early anterior signal that is sufficient (even when induced on the posterior side) to promote the consequent formation of all the anterior structures of the planarian head by inducing notum expression, which inhibits β-catenin-dependent Wnt signal transduction (Durant et al., 2019). These discoveries show that electrophysiological changes are important signals in the formation and growth of anatomical structures.

Our findings help explain how electrophysiological changes in cells can lead to broader tissue organizing phenomena by showing the inductive effect that increasing K^+ conductance can have on a broad number of developmental pathways, which is important for coordinating the organized formation of tissues and organs. Furthermore, the effect of the activity of this channel is broader than the traditional mechanisms of growth factor/morphogen signaling pathways, because it is not confined to specific signal transduction mechanisms; rather, it has variable broad effects, that is activation of several developmental signals in the adult fin (Fig. 1A) and the larva (Fig. 2A,B). We propose that the competence to activate different developmental pathways by electrophysiological changes is because the responding cells are either primed to activate them or the pathways are already active. It will be important to find out how this electrophysiological signal coordinates the activity of these developmental signals. In this regard, only few factors are known that regulate *shh* and *lef1* transcription. Thus, our finding that an electrophysiological mechanism is involved not only provides a new understanding of how electrophysiology acts as an inductive signal, it also may lead to the discovery of molecular mechanisms that control the expression of these mediators of important morphogen signals.

The scaling activity of Kcnk5b includes all the tissues of the entire appendages of the fish (Perathoner et al., 2014). Previous findings implicate broader intercellular electrophysiological gradients as a mechanism for tissue growth (Adams and Levin, 2013). Electrophysiological measurements of animal tissues show that electric fields are generated and are important *in vivo* (Borges et al., 1979; Jenkins et al., 1996; McGinnis and Jr., 1986), which suggests the existence of *in vivo* bioelectric information that regulates physiological

405 phenomena. However, from our transplantation experiments, we observe that the activation of
406 the growth program is cell autonomous (Fig. 3). Consequently, the question arises about how
407 the activity of this K^+-leak channel relates to a broad, coordinated phenotype of scaling the
408 several tissues of the fin. An answer is that the autonomous transcriptional program includes
409 morphogens. What is unclear is whether a limited number of cells in the fin control the
410 growth and organizing information so that Kcnk5b only needs to act on a limited number of
411 cell types, or whether Kcnk5b regulates proportional growth at multiple levels and that the
412 cell autonomous transcriptional response that we observe is one outcome of a combination of
413 intracellular and intercellular responses induced by Kcnk5b.

414 Changes in membrane potential from alterations in K^+ conductance are also associated
415 with the progression through the cell cycle (Blackiston et al., 2009; Urrego et al., 2014),
416 because K^+ channel activity increases at specific cell cycle phases (Urrego et al., 2014), and
417 inhibition of K^+ channel activity leads to cell cycle arrest in many different tissue cell types
418 (Blackiston et al., 2009). It is possible that this phenomenon explains part of Kcnk5b's ability
419 to promote allometric growth. We do not yet know whether other phenomena linked to the
420 activity of mammalian Kcnk5 [influence cell tonicity (Niemeyer et al., 2010), metabolic
421 acidosis and alkalinization (Warth et al., 2004), CO_2/O_2 chemosensing in retrotrapezoid
422 nucleus neurons (Flores et al., 2011) and apoptosis in lymphocytes and neurons (Göb et al.,
423 2015; Nam et al., 2011)] are involved in appendage scaling.

424 We previously showed that calcineurin inhibition shifts isometric growth to allometric
425 growth (Kujawski et al., 2014). Subsequently, Daane et al. showed that this effect is reversible
426 in that removal of calcineurin inhibitors restores isometric growth (Daane et al., 2018).
427 Together, these data implicate calcineurin as a molecular switch governing isometric versus
428 allometric growth control. Our findings provide a mechanism for how this switch acts to scale
429 the fish appendages by directly regulating the activity of Kcnk5b through the
430 dephosphorylation and phosphorylation of a specific serine (Fig. 7). The ability to mimic or
431 block calcineurin regulation of this K^+-leak channel (Fig. 5), whose activity levels directly
432 translate into the extent of allometric growth (Fig. 6), defines how calcineurin inhibition
433 expands clonal populations during fin regeneration (Tornini et al., 2016). However, as we
434 observed from both calcineurin inhibition (Kujawski et al., 2014) and from conditionally
435 inducing Kcnk5b activity (Fig. 5), the induced allometric growth of the entire fin is more than
436 expanding clonal populations, since the outcome is not tumorigenesis. Instead, the growth is
437 coordinated among all the tissues (Fig. 6G-I) (Kujawski et al., 2014; Perathoner et al., 2014),

438 and our finding that Kcnk5b activates several developmental pathways (Figs. 1,2,4) argues
439 that calcineurin activity acting on Kcnk5b regulates more than cell cycle progression.

440 An important next step is to learn how the calcineurin-Kcnk5b circuit is integrated into
441 the broader mechanisms that scale the appendages. Calcineurin is a Ca^{2+}-dependent enzyme
442 which suggests that intracellular Ca^{2+} is involved in scaling information. Ca^{2+} is a broad
443 second messenger that can activate several downstream Ca^{2+}-dependent enzymes, so broad
444 changes in its subcellular levels likely have multiple effects. It remains unclear whether there
445 is a specific intracellular distribution pattern that leads to calcineurin-mediated control of
446 scaling. It is also possible that Ca^{2+}-mediated activation of calcineurin—and consequent
447 restoration of isometric growth—is so dominant that other Ca^{2+}-mediated activities have little
448 effect.

449 Two mechanisms that regulate proportional growth of organs are vitamin D and Hippo
450 signaling. Increasing vitamin D signaling enhance the growth of the entire body, including the
451 fins (Han et al., 2019). We propose that vitamin D is a systemic body signal that ultimately
452 leads to the increase in Kcnk5b signaling. It is also possible that this hormone acts
453 independently of Kcnk5b. In *Drosophila,* the Hippo pathway regulates brain size and size of
454 the imaginal discs (Poon et al., 2016; Rogulja et al., 2008). Mice overexpressing a nuclear
455 version of the Hippo-signaling component Yap1 in the adult liver develop significantly
456 enlarged livers (Camargo et al., 2007; Dong et al., 2007). The Hippo signal transduction
457 pathway consists of several core components that can be regulated by different factors at
458 plasma membrane and within the cell (Yu and Guan, 2013), so there are several possible
459 nodes of interaction between of Kcnk5b and Hippo cascade. It is also possible the Hippo-
460 mediated transcription regulates *kcnk5b* expression or channel activity.

461 Connexin43 also regulates proportional growth of the fins, since mutations that reduce
462 the intercellular connectivity of connexin43 produce adult fins are half the size as the fins of
463 wild-type siblings (Hoptak-Solga et al., 2007; Iovine et al., 2005). The connective nature of
464 these intercellular junction proteins indicate that direct communication between intracellular
465 compartments of tissue cells is an important component of the scaling mechanism of the fins.
466 Our observation that Kcnk5b cell-autonomously activates the 7xTCFsamois-mCherry reporter
467 (Fig. 3) indicates that it is not due to intracellular transfer of K^+. It is still unclear whether the
468 disruption of intracellular trafficking of other ions (such as Na^+ or Ca^{2+}) or of other factors is
469 responsible for the connexin43's effect on scaling.

Kcnk5b's ability to activate the β-catenin-dependent Wnt reporter cell autonomously in different tissue types supports the conclusion that K^+ conductance has the potential to regulate developmental transcription in a broad range of tissues (Fig. 3B-D). The observation that neuronal cells in the brain and myocytes in the trunk muscle respond similarly to non-excitable cells elsewhere in the body suggests that even cells that harbor action potentials use K^+ conductance to regulate gene expression. Whether this mechanism contributes to the scaling of other organs or how other electrophysiological mechanisms that control membrane potential can have the same effect needs to be explored.

In conclusion, we show how a specific electrophysiological mechanism activates important morphogen pathways to scale tissues in different *in vivo* contexts. We propose the observed diversity in morphogen and growth factor expression to Kcnk5b activity explains why the increased activity of Kcnk5b produces the diverse transcriptional response in the different tissues associated with the observed coordinated outgrowth of the entire fin. Also, we show how changes in phosphorylation of S345 in the cytoplasmic C-terminus is regulated by calcineurin to directly control electrophysiological activity of the channel to scale the fin. Thus, we offer an *in vivo* paradigm in which membrane potential acts as potent regulator of coordinated developmental signaling and that this is how the two-pore K^+-leak channel Kcnk5b is able to scale the fish fin appendages.

Acknowledgements:

This work was supported by funding from ShanghaiTech University, the Deutsche Forschungsgemeinschaft Grant AN 797/4-1. We also wish to thank C. Bökel for scientific discussions.

Competing Interests

The authors declare that there are no competing interests.

Author contributions

C.Y., T.S., E.A.A.A., S.W., S.C., X.Y. Conducted experiments

M.W. Discussions, help with experimental design and analysis of electrophysiology data

A.E.A, K.G. Discussions, advice and financial support

C.A. Concept of the paper, designed experiments, conducted experiments, wrote the paper

Figures

Figure 1 Kcnk5b induces a partial developmental program in uninjured adult fins.

(**A**) qRT-PCR results of *shh* and *lef1* expression (**a**) and *aldh1α2*, *pea3* and *msxb* (**b**) from caudal fins of 6-month-old zebrafish comparing before (-HS) and 6 hours after (+HS) heat shock induction of the Tg[*hsp70*:*kcnk5b*-GFP] transgene in the caudal fins. (**B**) qRT-PCR results of *shh* and *lef1* expression (**a**) and *aldh1α2*, *pea3* and *msxb* (**b**) from caudal fins of 6-month-old zebrafish comparing before and 12-hours after heat-shock induction of the Tg[*hsp70*:*kcnk5b*-GFP] transgene in the caudal fins. (**C**) qRT-PCR results for several genes in the caudal fin from daily heat-shock pulse of Tg[*hsp70*:*knck5b*-GFP] over 3 days. (**D**) *in situ* hybridization experiments on fins show expression of *shh* (**a,b**) and *lef1* (**c,d**) before (**a,c**) and after (**b,d**) heat-shock induction of *kcnk5b*-GFP. (**E**) Cross sections through fin rays show expression of *shh* (**a,b**) and *lef1* (**c,d**) before (**a,c**) and after (**b,d**) heat-shock induction of *kcnk5b*-GFP. (**F**) Representative images of Western blots show expression of Shh, Lef1 and β-catenin before and 3 days after 10-minute daily heat-shock induction of *kcnk5b*-GFP in the fin. (**G**) Graphed measurements results of Western blots. (**H**) Immunohistochemistry stainings for (Kcnk5b-GFP) GFP (**a,b**: green), β-catenin (**c,d**: red) and DAPI (**e,f**: blue) of fin cross sections of transgenic *kcnk5b*-GFP animals without heat shock (**a,c,e,g,i**) or after heat shock (**b,d,f,h,j**). White boxes in **g** and **h** show location of magnified panels of **i** and **j**. Overlapping DAPI and β-catenin staining indicated by white arrows. (**I**) Graphed measurements of DAPI stained nuclei containing staining of β-catenin. (**J**) Graphed measurements of β-catenin fluorescence intensity of stained sections. Scale bars are 50 μm (D), 1 mm (E), 10 μm (H). The data for each experiment represent an N of 3 or more, which each N having 2 or more replicates. Student's T-test used for the tests of significance between indicated experimental groups.

Figure 2: Kcnk5b induces *shh* and *lef1* in zebrafish larva.

(**A**) Comparison of gene expression from zebrafish larva harboring Tg[*hsp70*:*knck5b*-GFP] before and 6 hours after heat-shock (HS) induction. (**B**) Double transgenic fish harboring Tg[*hsp70*:*kcn5b*-GFP] and Tg[7x*TCFsamois*:mCherry] either before heat shock (**a-c**) or 12 hours after heat shock (**d-f**). (**Bg**) Measurements of mCherry intensity levels of non-transgenic (non-tg), *kcnk5b*-transgenic (*kcnk5b*) fish and transgenic fish harboring the β-catenin-dependent Wnt 7xTCF*samois*:mCherry reporter (7xTCF) before and 12 hours after heat shock.

(**C**) Cross sections through the trunks of non-transgenic (**a-d**) and single- (**e-h**) and double-transgenic (**i-l**) fish lines after heat shock. (**D**) Measurements from dorsal to ventral of the caudal finfold of Tg[7xTCF*samois*:mCherry] and Tg[7xTCF*samois*:mCherry]X Tg[*hsp70:kcnk5b*] sibling larva after heat shock. Scale bars are 100µm (**B**) and 20µm (**C**). The data for each experiment represent an N of 3 or more, which each N having 3 or more replicates. Student's T-test used for all test of significance between the indicated experimental groups.

Figure 3: Kcnk5b induces β-catenin-dependent transcription in several tissues in a cell autonomous manner.

(**A**) Diagram of transplantation procedure and possible cell-autonomous and non-cell-autonomous outcomes on the expression of the *7xTCFsamois*:mCherry reporter after heat-shock induction of the *kcnk5b*-GFP transgene. (**B**) Transplantation experiments of donor cells from double transgenic fish harboring Tg[*hsp70*:*kcnk5b*-GFP] and Tg[7xTCF*samois*:mCherry] into host embryos harboring only the Tg[7xTCF*samois*:mCherry]. The head (**a**) eye (**e**) trunk (**i**) and finfold (**m**) of mosaic larva before heat shock induction of *kcnk5b*-GFP expression. Head (**b-d**), eye (**f-h**), trunk (**j-l**) and finfold (**n-p**) 24 hours after heat shock. (**C**) Bright field images of the head (**a,d**), jaw area (**g**) border tissue of otic vesicle (**j**) and trunk (**o,r**); *kcnk5b*-GFP expression (**b,e,h,k,p,s**) and 7xTCF*samois*: mCherry expression (**c,f,i,l,q,t**). (**D**) Total number of positive cells counted in the tissues of all mosaic larva for all mCherry-positive cells (open red circle), all *kcnk5b*-GFP-positive cells (open green triangle) and all double positive cells (open blue squares).

Figure 4 Kcnk5b channel activity regulates developmental gene transcription in mammalian cells.

(**A**) FRET-FLIM images after measuring the life time of CFP of the K^+ FRET reporter KIRIN (Shen et al., 2019). The color images indicate the differences in CFP fluorescence lifetime of the K^+ FRET reporter KIRIN in HEK293T (HEK) cells. Assigned rainbow of colors in the delineated cytoplasm depict the range of numeric values of nanoseconds (ns) of the detected fluorescent lifetime for CFP. Red represents longer lifetime values. Blue represents shorter lifetime values, and the other colors represent intermediary lifetime values. (**a**) Composite image of all lifetime values of the KIRIN K^+ reporter in control cells transfected with

mCherry. (**b**) Image of low lifetime values in a control cell. (**c**) Image of high lifetime values in a control cell. (**d**) Composite image of all lifetime values of the KIRIN K^+ reporter in cells expressing *kcnk5b*-mCherry. (**e**) Image of low lifetime values in cells expressing *kcnk5b*-mCherry. (**f**) Image of high lifetime values in cells expressing *kcnk5b*-mCherry. (**g**) Compared to GFP-transfected HEK cells, cells transfected with *kcnk5b*-mCherry show an increase in CFP lifetime due to reduction in intracellular K^+. (**Ba**) qRT-PCR for SHH and LEF1 in HEK cells. (**Bb**) qRT-PCR for ALDH1a2, PEA3 and MSX1 in HEK cells. **(C**) qRT-PCR for indicated genes in HEK cells expressing GFP, *kcnk9*-GFP or *kcnk10*-GFP 24 hours after transfection. (**D**) qRT-PCR results in HeLa cells expressing either GFP or *kcnk5b*-GFP 24 hours after transfection. (**E,F)** qRT-PCR results in N2A cells expressing either GFP or *kcnk5b*-GFP 24 hours after transfection. (**G**) qRT-PCR results in Mcf7 cells expressing either GFP or *kcnk5b*-GFP 24 hours after transfection. Student's T-test was used for tests of significance and the levels of significance are indicated between the experimental groups.

Figure 5 Calcineurin functionally interacts and regulates channel activity of Kcnk5b. (**A**) Diagram of hypothetical interaction between Calcineurin (CaN) and Kcnk5b at a consensus calcineurin binding site (LVIP) in Kcnk5b. (**B**) Whole-cell patch clamp of HEK293T (HEK) cells expressing the indicated zebrafish proteins: Calcineurin-mCherry and Kcnk5b-GFP. (**C**) Whole-cell patch-clamp results of cells expressing zebrafish Kcnk5b-GFP and treated either with DMSO or the calcineurin inhibitor FK506. (**D**) Diagram shows mutant Kcnk5b with altered amino acids at putative calcineurin binding site and graph of the Patch-clamp results of the wild-type zebrafish Kcnk5b channel (Kcnk5bLVIP) or mutant Kcnk5b (Kcnk5bmutVATA) lacking the putative calcineurin binding site. Each construct is expressed either with or without calcineurin (CaN). (**E)** qRT-PCR for SHH in HEK cell lines stably expressing either GFP or Kcnk5b-GFP and transfection with calcineurin-mCherry (CaN). **(F**) qRT-PCR for PEA3 in HEK cell lines stably expressing either GFP or Kcnk5b-GFP and transfection with calcineurin-mCherry (CaN). (**G**) qRT-PCR of SHH expression HEK cells after transfection either with GFP, *kcnk9*-GFP or *kcnk10*-GFP with or without calcineurin. (**H**) qRT-PCR of PEA3 expression HEK cells after transfection either with GFP, *kcnk9*-GFP or *kcnk10*-GFP with or without calcineurin. The electrophysiology measurements (**B-D**) are averages with SEM. (**E-G**) Graph panels show averages. The data for each experiment represent an N of 3 or more, which each N having 2 or more replicates. Student's T test was used to determine the indicated significance (P) values.

Figure 6 Regulation of Kcnk5b controls scaling of the fin

(**A**) Diagram of Kcnk5b channel showing proposed Serine345Proline346 calcineurin dephosphorylation site adjacent the calcineurin-interaction site (LVIP). Mutation of S345 to alanine (A) mimics dephosphorylation. (**B)** Whole-cell patch-clamp results of HEK239T (HEK) cells transfected with zebrafish wild-type channel (Kcnk5bS345) or the dephospho-mimic mutant (KcnkS345A) either with or without calcineurin (CaN). (**C**) Diagram of serine (S) to glutamic acid (E) substitution to mimic phosphorylation of Kcnk5b. (**D**) Whole-cell patch-clamp measurements for wild-type Kcnk5b and mutant Kcnk5b harboring a Serine345 to glutamic acid either with or without calcineurin (CaN). (**E**) Graph displays different growth rates of the regenerating caudal fin lobes of the indicated transgenic fish lines. Body length of each fish was used to standardize the fin length measurements (fin-to-body ratio). (**F**) Caudal fin of Tg[*hsp70:kcnkbS345A*] transgenic fish after regeneration of ventral lobe. (**G**) Caudal fin of Tg[*hsp70:kcnk5bS345*] transgenic fish after regeneration of ventral lobe. (**H**) Caudal fin of Tg[*hsp70:kcnk5bS345E*] transgenic fish after regeneration of ventral lobe. (**I**) Graph of fin-to-body ratios of the unamputated lobes of the indicated transgenic fish lines at 33 days of the same fish as in (F). (**J**) Graph of the measured bone segment lengths of the unamputated caudal fin lobes from non-transgenic, Tg[*hsp70*:*kcnk5bS345EA*], and Tg[*hsp70*:*kcnk5bS345E*] fish. The measurements of each segment extend from the proximal base of the fin (segment 0) to distal tip of the lobe (segment 34). $p<0.025$ value is between Tg[*hsp70*:*kcnk5bS345E*] and non-Tg fish. The data for each experiment represent an N of 3 or more, which each N having 3 or more replicates. The electrophysiology measurements (panels **B,D**) are represented as averages with SEM. Significance values shown in the graphs were measured by students t-tests (E, I, J) are represented as averages and SD. The scale bars equal 2 mm (F-H).

Figure 7: Model of calcineurin regulation of Kcnk5b-mediated activation of developmental programs. Kcnk5b activation results in reduced cytoplasmic K^+, which is sufficient to induce the transcription of the *shh* ligand and *lef1* transcription factor (β-catenin-dependent Wnt signaling) as well as components of other developmental pathways to induce coordinated allometric growth of the tissues of the fish fin appendage. Scaling information from the body or local tissues in the fin activate calcineurin so that it dephosphorylates Kcnk5b on S345 to reduce its K^+-channel activity, which results in isometric growth of the fin.

References:

Adams, D.S., and Levin, M. (2013). Endogenous voltage gradients as mediators of cell-cell communication: strategies for investigating bioelectrical signals during pattern formation. Cell Tissue Research *352*, 95-122.

Andersen, E.D., Krasilnikoff, P.A., and Overvad, H. (1971). Intermittent muscular weakness, extrasystoles, and multiple developmental anomalies. A new syndrome? Acta Paediatr Scand *60*, 559-564.

Baer, M.L., and Colello, R.J. (2016). Endogenous bioelectric fields: a putative regulator of wound repair and regeneration in the central nervous system. Neural Regneration Research *11*, 861-864.

Balciunas, D., Wangensteen, K.J., Wilber, A., Bell, J., Geurts, A., Sivasubbu, S., Wang, X., Hackett, P.B., Largaespada, D.A., McIvor, R.S., *et al.* (2006). Harnessing a high cargo-capacity transposon for genetic applications in vertebrates. PLoS Genetics *2*, e169.

Bartel, D.P., Sheng, M., Lau, L.F., and Greenberg, M.E. (1989). Growth factors and membrane depolarzation activate distinct programs of early response gene expressoin: dissociation of fos and jun induction. Genes & Development *3*, 304-313.

Blackiston, D.J., McLaughlin, K.A., and Levin, M. (2009). Bioelectric controls of cell proliferation: Ion channels, membrane voltage and the cell cycle. Cell Cycle *8*, 3527-3536.

Borgens, R.B., J. W. Vanable, J., and Jaffe, L.F. (1977). Bioelectricity and Regeneration. I Initiation of Frog Limb Regeneration by Minute Currents. Journal of Experimental Zoology *200*, 403-416.

Borges, R.B., Joseph W. Vanable, J., and Jaffe, L.F. (1979). Reduction of Sodium Dependent Stump Currents Disturbs Urodele Limb Regeneration. Journal of Experimental Zoology *208*, 377-386.

Brand, M., Granato, M., and Nüsslein-Volhard, C. (2002). Keeping and raising zebrafish. In Zebrafish: a Practical Approach, C. Nüsslein-Volhard, and R. Dahm, eds. (Oxford University Press), pp. 7-38.

Camargo, F.D., Gokhale, S., Johnnidis, J.B., Fu, D., Bell, G.W., and al., e. (2007). YAP1 increases organ size and expands undifferentiated progenitor cells. Current Biology *17*, 2054-2060.

Canun, S., Perez, N., and Beirana, L.G. (1999). Andersen syndrome autosomal dominant in three generations. Am J Med Genet *85*, 147-156.

Chow, R.L., Altmann, C.R., Lang, R.A., and Hemmati-Brivanlou, A. (1999). Pax6 induces ectopic eyes in a vertebrate. Development *126*, 4213-4222.

Daane, J.M., Lanni, J., Rothenberg, I., Seebohm, G., Higdon, C.W., Johnson, S.L., and Harris, M.P. (2018). Bioelectric-calcineurin signaling module regulates allometric growth and size of the zebrafish fin. Scientific Reports *8*, 10391.

Dahal, G.R., Rawson, J., Gassaway, B., Kwok, B., Tong, Y., Ptacek, L.J., and Bates, E. (2012). An inwardly rectifying K+ channel is required for patterning. Development *139*, 3653-3664.

Dong, J., Feldmann, G., Huang, J., Wu, S., Zhang, N., Comerford, S.A., Gayyed, M.F., Anders, R.A., Maitra, A., and Pan, D. (2007). Elucidation of a universal size-control mechanism in Drosophila and mammals. Cell *130*, 1120-1133.

Durant, F., Bischof, J., Fields, C., Morokuma, J., LaPalme, J., Hoi, A., and Levin, M. (2019). The role of early bioelectric signals in the regeneration of planarian anterior/posterior polarity. Biophysical Journal *116*, 948-961.

Flores, C., Cid, L., Niemeyer, M., and Sepulveda, F. (2011). B Lymphocytes taken to task: a role for a background conductance K2p K+ channel in B cells. Focus on "Expression of TASK-2 and its up-regulation by B cell receptor stimulation in WEJI-231 mouse immature B cells". American Journal of Physiology Cell Physiology *300*, C976-C978.

677 Geremia, N.M., Gordon, T., Burshart, T.M., Abdulhakeem A. Al, M., and Verge, V.M.K. (2007).
678 Electrical Stimulation Promotes Sensory Neuron Regeneration and Growth-associated Gene
679 Exrpression. Experimental Neurobiology *205*, 327-359.

680 Göb, E., Bittner, S., Bobak, N., Kraft, P., Göbel, K., Langhauser, F., Homola, G.A., Brede, M., Budde,
681 T., Meuth, S.G., *et al.* (2015). The two-pore domain potassium channel KCNK5b deteriorates the
682 outcome in ischemic neurodegeneration. Pfluger Archive-European Journal of Physiology *467*, 973-
683 987.

684 Goldstein, S.A.N., Bockenhauer, D., O'Kelly, I., and Zilberberg, N. (2001). Potassium leak channels
685 and the KCNK family of two-P-domain subuints. Nature Reviews Neuroscience *2*, 176-184.

686 Grigoriu, S., Bond, R., Cossio, P., Chen, J.A., Ly, N., Hummer, G., Page, R., Cyert, M.S., and Peti, W.
687 (2013). The molecular mechanisms of substrate engagement and immunosuppressant inhibition of
688 calcineurin. Plos Biology *11*, e1001492.

689 Halder, G., Callaerts, P., and Gehring, W.J. (1995). Induction of ectopic eyes by targeted expression of
690 the eyeless gene in Drosophila. Science *267*, 1788-1792.

691 Han, Y., Chen, A., Umansky, K.-B., Oonk, K.A., Choi, W.-Y., Dickson, A.L., Ou, J., Cigiola, V.,
692 Yifa, O., Cao, J., *et al.* (2019). Vitamin D stimulates cardiomyocyte proliferation and controls organ
693 size and regeneration in zebrafish. Developmental Cell *48*, 853-863.

694 Hoptak-Solga, A.D., Klein, K.A., DeRosa, A.M., White, T.W., and Iovine, M.K.-. (2007). Zebrafish
695 short fin mutations in connexin4 lead to aberrant gap junctional intercellular communication. FEBS
696 letters *581*, 3297-3302.

697 Iovine, M.K., Higgins, E.P., Hindes, A., Coblitz, B., and Johnson, S.L. (2005). Mutations in
698 *connextin43* (*GJA1*) perturb bone growth in zebrafish fins. Developmental Biology *278*, 208-219.

699 Jenkins, L.S., Duerstock, B.S., and Borges, R.B. (1996). Reduction of the Current of Injury Leaving
700 the Amputation Inhibits Limb Regeneration in the Red Spotted Newt. Developmental Biology *178*,
701 251-262.

702 Kujawski, S., Lin, W., Kitte, F., Börmel, M., Fuchs, S., Arulmozhivarman, G., Vogt, S., Theil, D.,
703 Zhang, Y., and Antos, C.L. (2014). Calcineurin regulates coordinated outgrowth of zebrafish
704 regenerating fins Developmental Cell *28*, 1-15.

705 Lanni, J.S., Peal, D., Ekstrom, L., Chen, H., Stanclift, C., Bowen, M.E., Mercado, A., Gamba, G.,
706 Kahle, K.T., and Harris, M.P. (2019). Integrated K+ channel and K+Cl- cotransporter function are
707 required for the coordination of size and proportion during development. Dev Biol *456*, 164-178.

708 Levin, M. (2014). Molecular bioelectricity: how endogenous voltage potentials control cell behavior
709 adn instruct pattern regualtion in vivo. Molecular Biology of the Cell *25*, 3835-3850.

710 Marcoux, A.A., Garneau, A.P., Frenette-Cotton, R., Slimani, S., Mac-Way, F., and Isenring, P. (2017).
711 Molecular features and physiologal roles of K+-Cl- cotransporter 4. BBA-General Subjects *1861*,
712 3154-3166.

713 McCaig, C.D., Rajnicek, A.M., Song, B., and Zhao, M. (2005). Controlling Cell Behavior Electrically:
714 Current Views and Future Potential. Physiol Rev *85*, 943-978.

715 McGinnis, M.E., and Jr., J.W.V. (1986). Electrical Fields in Notophthalmus viridescens Limb Stumps.
716 Developmental Biology *116*, 184-193.

717 McLaughlin, K.A., and Levin, M. (2018). Bioelectric signaling in regeneration: Mechanismsof ionic
718 controls of growth and form. Developmental Biology *433*, 177-189.

719 Messerli, M.A., and Graham, D.A. (2011). Extracellular electrical fields direct wound healing and
720 regeneration. The Biological Bulletin *221*, 72-92.

721 Moro, E., Ozhan-Kizil, G., Mongera, A., Beis, D., Wierzbicki, C., Young, R.M., Bournele, D.,
722 Domenichini, A., Valdivia, L.E., Lum, L., *et al.* (2012). In vivo Wnt signaling tracing through a
723 transgenic biosensor fish reveals novel activity domains. Developmental Biology *366*, 327-340.

Morokuma, J., Blackiston, D., Adams, D.S., Seebohm, G., Trimmer, B., and Levin, M. (2008). Modulation of potassium channel functions confers a hyperproliferative invasive phenotype on embryonic stem cells. Proceeding of the National Academy of Sciences USA *105*, 16608-16613.

Nam, J., Shin, D., Zheng, H., Lee, D., Park, S., Park, K., and Kim, S. (2011). Expression of TASK-2 and its upregulation by B cell receptor stimulation in WEHI-231 mouse immature B cells. American Journal of Physiology Cell Physiology *300*, C1013-1022.

Niemeyer, M., Cid, L., Pena-Münzenmayer, G., and Sepulveda, F. (2010). Modulation of the two-pore domain acid-sensitive K+ channel TASK-2 (KCNK5) by changes in cell volume. Journal of Biological Chemistry *276*, 43166-43174.

Pai, V.P., Aw, S., Shomrat, T., Lemire, J.M., and Levin, M. (2012). Transmembrane voltage potential controls embryonic eye patterning in Xenopus laevis. Development *139*, 313-323.

Pai, V.P., Lemire, J.M., Chen, Y., Lin, G., and Levin, M. (2015). Local and long-range endogenous resting potential gradients antagonistically regulate apoptosis and proliferation in the embryonic CNS. International Journal of Developmental Biology *59*, 327-340.

Perathoner, S., Daane, J.M., Henrion, U., Seebohm, G., Higdon, C.W., Johnson, S.L., Nüsslein-Volhard, C., and Harris, M.P. (2014). Bioelectric signaling regulates size in zebrafish fins. PLoS Genetics *10*, e1004080.

Poon, C.L.C., Mitchell, K.A., Kondo, S., Cheng, L.Y., and Harvey, K.F. (2016). The hippo pathway regulates neuroblasts and brain size in Drosophila melanogaster. Current Biology *26*, 1034-1042.

Rogulja, D., Rauskolb, C., and Irvine, K.D. (2008). Morphogen control of Wing Growth troguh the fat signaling pathway. Developmental Cell *15*, 309-321.

Sansone, V., Griggs, R.C., Meola, G., Ptacek, L.J., Barohn, R., Iannaccone, S., Bryan, W., Baker, N., Janas, S.J., Scott, W., *et al.* (1997). Andersen's syndrome: a distinct periodic paralysis. Ann Neurol *42*, 305-312.

Shattock, M.J., Ottolia, M., Bers, D.M., Blaustein, M.P., Boguslavskyi, A., Bossuyt, J., Bridge, J.H.B., Chen-Izu, Y., Clancy, C.E., Edwards, A., *et al.* (2015). Na+/Ca2+ exchange and Na+/K+-ATPase in the heart. Journal of Physiology *593.6*, 1361-1382.

Shen, Y., Wu, S.-Y., Rancic, V., Aggarwal, A., Qian, Y., Miyashita, S.-I., Ballanyi, K., Campbell, R.E., and Dong, M. (2019). Genetically encoded fluorescent indicators for imaging intracellular potassium ion concentration. Communications Biology *2*.

Stewart, S., Bleu, H.K.L., Yette, G.A., Henner, A.L., Braunstein, J.A., and Stankunas, K. (2020). longfin causes *cis*-ectopic expression of the *kcnh2a ether-a-go-go* K+ channel to autonomously prolong fin outgrowth. bioRxiv

Sundelacruz, S., Levin, M., and Kaplan, D.L. (2009). Role of Membrane Potential in the Regulation of Cell Proliferation and Differentiation. Stem Cell Review and Reports *5*, 231-246.

Tawil, R., Ptacek, L.J., Pavlakis, S.G., DeVivo, D.C., Penn, A.S., Ozdemir, C., and Griggs, R.C. (1994). Andersen's syndrome: potassium-sensitive periodic paralysis, ventricular ectopy and dysmorphic features. Ann Neurol *35*, 326-330.

Tornini, V.A., Puliafito, A., Slota, L.A., Thompson, J.D., Nachtrab, G., Kaushik, A.-L., Kapsimali, M., Primo, L., Talia, S.D., and Poss, K.D. (2016). Live Monitoring of Blastema Cell Contributions during Appendage Regeneration. Current Biology *26*, 2981-2991.

Urrego, D., Tomczak, A.P., Zahed, F., Stühmer, W., and Pardo, L.A. (2014). Potassium channels in cell cycle and cell proliferation. Philosophical Transactions of the Royal Society B *369*, 20130094.

Warth, R., Barriere, H., Meneton, P., Bloch, M., Thomas, J., Tauc, M., Heitzmann, D., Romeo, E., Verrey, F., Mengual, R., *et al.* (2004). Proximal renal tubular acidosis in TASK2 K+ channel-deficient mice reveals a mechanism for stabilizing bicarbonate transport. Proceeding of the National Academy of Scinences USA *101*, 8215-8220.

771 Yasuda, I. (1974). Mechanical and Electrical Callus. Clinical Studies. Annals New York Academy of
772 Sciences, 457-465.

773 Yoon, G., Quitania, L., Kramer, J.H., Fu, Y.H., Miller, B.L., and Ptacek, L.J. (2006a). Andersen-Tawil
774 syndrome: definition of a neurocognitive phenotype. Neurology *66*, 1703-1710.

775 Yoon, G., Tristani-Firouzi, M., Etheridge, S.P., Quitania, L., Kramer, J.H., Miller, B.L., Fu, Y.H., and
776 Ptacek, L.J. (2006b). Andersen-Tawil syndrome: prospective cohort analysis and expansion of the
777 phenotype. Am J Med Genet *140A*, 312-321.

778 Yu, F.-X., and Guan, K.-L. (2013). The Hippo pathway: regulators and regulations. Genes &
779 Development *27*, 355-371.

780 Zaritsky, J.J., Eckman, D.M., Wellman, G.C., Melson, M.T., and Schwarz, T.L. (2000). Targeted
781 disruption of Kir2.1 and Kir2.2 genes reveals the essential role of the inwardly rectifying K^+ current in
782 K^+-mediated vasodilation. Circulation Research *87*, 160-166.

783 Zhao, M., Pu, J., Forrester, J.V., and McCaig, C.D. (2002). Membrane lipids, EGF receptors, and
784 intracellular signals colocalize and are polarized in epithelial cells moving directionally in a
785 physiological electric field. FASEB Journal *16*.

786

Material and Methods

Cloning

Constructs were designed either using standard restriction enzyme or by homologous recombination methods. *kcnk5b* cDNA was isolated by RT-PCR from regenerating adult fin cDNA library and cloned into MCS region of pcDNA6-myc-6xHIS-tag plasmid (Invitrogen) or pBluescript harboring the *hsp70* zebrafish promoter and GFP coding sequence surrounded by 2 miniTol2 sites. Mutagenesis of the Serine345 codon of Kcnk5b was performed using QuikChange Mutagenesis kit (Agilent).

Zebrafish Husbandry

AB strain fish were raised in 10L tanks with constantly flowing water, 26ºC standard light-dark cycle (Brand et al., 2002) in either a Schwarz (DFG-Center for Regeneration, TU Dresden) or HaiSheng aquarium (ShanghaiTech University) systems. Transgenic lines were created by injecting 300 µg of each construct together with mRNA of Tol2 transposase (Balciunas et al., 2006). Fish embryos and larva were raised in 1xE3 medium (5mM NaCl, 0.17mM KCl, 0.33mM $CaCl_2$, 0.33mM $MgSO_4$, 10^{-5}% Methylene Blue) until 10-12dpf, then transferred to aquarium water tanks to grow. Transgenic lines established by screening for GFP expression after heat shock. Experiments used male and female fish equally. Fish experiments were compliant to the general animal welfare guidelines and protocols approved by legally authorized animal welfare committees (Technische Universität Dresden, Landesdirektion Dresden, and ShanghaiTech University, ShanghaiTech Animal Welfare Committee).

Heat shock induction of transgenes

Parents of heat-shock-driven transgenic lines were either outcrossed to same-strain wild-type fish or to fish harboring Tg[7xTCF*samois*:mCherry] transgene. Progeny were collected in 1xE3 and raised at 28^0C. Carriers were confirmed positive for their respective transgenes by a single heat shock at 37^0C for 1 hour. For embryo experiments, heat shock was at 12hpf in 37ºC E3 medium for 30 min. For larva the heat shock was in 37ºC E3 medium for 30 min. at 2 dpf. For adult fin, 6 month-old fish underwent a daily heat-chock regimen: first, sedated in 0.04% tricane in aquarium water, then placed in conical tubes containing 0.04% tricane in aquarium water to allow continued gill movement in oxygenated water and allow the caudal fins to be exposed to 37ºC water for 7 min. After heat shocking the caudal fin, the fish were returned to flowing aquarium water and monitored daily.

Immunohistochemistry

After 4 hours, larvae were euthanized in 1% Mesab, fixated in 4%PFA/1xPBS and embedded in 1% agarose (CryoStar NX50, Thermofisher) before cryosectioning. 10 µm sections were mounted on glass slides (Brand, Thermofisher) and dried. The tissue freezing medium (Leica) was removed in ddH_2O for 10min. Sections were permeabilized in 0.1%Triton-X for 5min and incubated in 1% BSA/1xPBS/0.1%Tween-20 (PBST) at room temperature for 30min. Sections were incubated in a mouse-anti-GFP (Invitrogen, MA5-15349), rabbit-anti-mCherry antibody (Invitrogen, P5-34974) solution (1:2000 dilution) in PBST at 4ºC overnight. The primary antibody solution was replaced by a goat-anti-mouse-GFP (Abcam, ab150113), goat-anti-rabbit-mCherry secondary antibody (Abcam, ab 150078) solution (1:2000 dilution) in PBST and incubated at RT in the dark for 60 min. The secondary antibody solution was then replaced with DAPI solution (Roche, 10236276) in the dark at room temperature for 5 min. DAPI were washed away in 1xPBS. Coverslips were mounted with a 40% glycerol solution and sealed with nail polish. The sections were visualized using an LSM710 confocal (Zeiss) with ZENBlue software (Zeiss). Images were processed with Fiji software.

Cell Transplantations

Transgenic fish lines [*hsp70*:*kcnk5b*-GFP] and [7xTCF*samois*:mCherry] were inbred for 20-30 min before embryos were collected in E3. The parents were confirmed to be positive for the respective transgene to ensure the highest number of embryos positive for the transgene. The embryos were left to develop in E3 for 3-3.5 hours at 28^0C until the blastula stage. Embryos were then placed in agarose ridges for easy access under a Zeiss stereomicroscope and cells from the [*hsp70*:*kcnk5b*-GFP] embryos were isolated by air suction via a glass needle mounted on a Precision Instruments piston. The [*hsp70*:*kcnk5b*-GFP] cells were then transplanted into the [7xTCFsamois:mCherry] embryos. The transplants were carefully moved from the agarose into clean 90mm dishes with fresh E3 (+/- 20-25 per dish) and incubated at 28^0C. Embryos hatched about 3 days after transplantation. They were directly heat shocked for 1 hour at 37^0C. Four hours after heat shock, larvae were embedded into 1% low melting agarose (Sigma-Aldrich-Aldrich, A9414-250G) supplemented with Mesab in 35mm glass bottom confocal dishes (Cellvis: D35-20-1-N) and turned to their side. Visualized with a LSM710 confocal argon laser microscope (Zeiss) with ZENBlue software (Zeiss).

In situ hybridization

mRNA probes were made from RT-PCR products isolated from 2 dpf zebrafish embryos. The primer sequences for generating the probes are F- *shha*:5'- TGCGGCTTTTGACGAGAG TGC-3'R-shha: 5'- GGTAATACGACTCACTATAGGG TTTCCCGCGCTGTCTGCCG-3' F-lef1 : 5'-GAGTTGGACAGATGACCCCTCCTC-3'; R-lef1：5'-GGTAATACGACTCA CTATAGGGGCAGACCATCCTGGGTAAAG-3'. *in vitro* transcription reagents are from Promega. Isolated fish fins were surgically isolated and incubated in 4% PFA in 1xPBS at 4ºC overnight with gentle rocking. Samples were subsequently washed 5 times in 1xPBS and then dehydrated by incubation for 15 min in a graded series of increasing methanol/1xPBS solutions (25%, 50%, 75%, 3x 100%) on ice. Fins were then incubated in 100% methanol for ≥2hrs at -20ºC. Samples were then rehydrated using the reversed dehydration series of methanol/1xPBS solutions). Samples were then incubated more than 4x in 1xPBS to remove all methanol, and subsequently incubated in 10µM Proteinase K for 10 min at RT. Samples were then incubated 20 min. in 4% PFA/1xPBS to inactivate the Proteinase K. Samples were incubated in 1xPBS 6x 10 mins to remove the PFA, then incubated in pre-hybridization buffer for 2 hours at 65C. Samples were subsequently incubated in the hybridization solution containing 200ng/ml of each mRNA probe ≥ 14 hrs at 65ºC. Samples then were washed with successive wash steps to remove unbound probe and prepare for antibody incubation: twice 2xSSC/50% deionized formalin at 65ºC, twice 2xSSC/25% deionized formalin at 65ºC, 2xSSC at 65ºC, twice 0.2xSSC at RT, 6 times 1xPBST (1xPBS with Tween-20), once in blocking solution [2% Bovine albumin (Sigma-Aldrich, A3294-100G), 2% Sheep Serum (Meilunbio, M134510)] at RT for 4 hours. Samples were incubated with Anti-digoxigenin-AP Fab Fragment (Sigma-Aldrich, 11093274910) in blocking solution ≥14 hrs at 4ºC. Samples were then washed 6 times with 1xPBST, subsequently incubated in [0.1 M Tris-HCl, pH 9.5, 0.1 M NaCl, 0.05 M $MgCl_2$] 3 times for 30 min, and then in Nitro Blue Tetrazolium (Sigma-Aldrich, N6639-1G) and 5-bromo-4-chloro-3-indolyl phosphate (Sigma-Aldrich, 136149) in [0.1 M Tris-HCl, pH 9.5, 0.1 M NaCl, 0.05 M $MgCl_2$] at RT ≥8hrs. Samples images under Stemi508 stereoscope (Zeiss) with Axiocam ERc5s digital color camera (Zeiss) and Zen2.3 software (Zeiss).

Immunohistochemistry

Zebrafish fins or larvae euthanized in 1% Mesab were fixed in 4%PFA/1xPBS and embedded in 1% agarose or tissue freezing medium (Leica, 14020108926) on dry ice. (CryoStar NX50,

887 Thermofisher) before cryosectioning. 10 μm sections were mounted on glass slides (Titan,
888 02036398) and dried. The tissue freezing medium (Leica) was removed in ddH_2O for 10min.
889 Sections were permeabilized in 0.1%Triton-X for 5min and incubated in 1%
890 BSA/1xPBS/0.1%Tween-20 (PBST) at room temperature for 30min. Sections were incubated
891 in a mouse-anti-GFP (Invitrogen, MA5-15349), (1:400) Anti-β-catenin (Cell Signaling,
892 9562L), rabbit-anti-mCherry antibody (Invitrogen, P5-34974) solution (1:2000 dilution) in
893 PBST at 4ºC overnight (>12 hours). The primary antibody solution was replaced by a goat-
894 anti-mouse-GFP (Abcam, ab150113), goat-anti-rabbit-mCherry secondary antibody (Abcam,
895 ab 150078) solution (1:2000 dilution) in PBST and incubated at RT in the dark for 60 min.
896 The secondary antibody solution was then replaced with DAPI solution (Roche, 10236276) in
897 the dark at room temperature for 5 min. DAPI were washed away in 1xPBST 3x 5-min
898 incubations at RT. Coverslips (Titan, 02036401) were mounted with a 40% glycerol solution
899 and sealed with nail polish. The sections were visualized using an LSM710 upright scanning
900 confocal (Zeiss) or a LSM880 inverted scanning confocal (Zeiss) with ZENBlue software
901 (Zeiss). Images were processed with Fiji software.
902

903 *β-catenin nuclear analysis on IHC cross sections of fins*

904 Using Fiji ImageJ, multiple nuclei of cells in IHC fin cross section image of control fins were
905 manually measured, and a mean mRFP fluorescence intensity value was calculated. This
906 mean value was used as the baseline for assessing nuclear β-catenin levels. β-catenin nuclear
907 values for all the nuclei in each cross section were assessed with ImageJ by splitting the
908 combined images of β-catenin and DAPI and using DAPI to have Fiji ImageJ define and
909 select all nuclei in the image. The nuclear β-catenin levels were determined in selected nuclei
910 by intensity analysis in Fiji ImageJ, which provided a numeric value for the β-catenin channel
911 in all the nuclei of each section.
912

913 *qRT-PCR*

914 The cDNA that was used for qRT-PCR was extracted from the HEK293T cells and zebrafish.
915 The mRNA was isolated using Tri-Reagent (CWBio, 03917). Then 1μg mRNA was used for
916 the reverse transcription to cDNA using 4x gDNA wiper Mix, 5x HiScript III qRT SuperMix
917 (Vazyme, L/N 7E350C9). qRT-PCR was performed using 2x ChamQ Universal SYBR qPCR
918 Master Mix (Vazyme, L/N TE342F9) with QuantStudio3 machine (Thermofisher). The cycle

procedure was at 50.0°C for 2 min, 95.0°C for 10 min in the stage 1; 95.0°C for 15 s, 60.0°C for 20s for 40 routine in the stage2; 95.0°C for 15s, 60.0°C for 1 min, 95.0°C for 15s in the Melt Curve. The data was analyzed in the ΔΔCt method.

Cell Culture

All cell culture lines were incubated at 37ºC, 5% CO2, 95% humidity in incubators (Thermofisher, FORMA STERI-CYCLE i160). Cell were split to 50% density and transfected with Lipofectamine™ (Invitrogen, 11668-019) 12 hours later. Expression for the transfected constructs was evaluated by expression of fluorescent marker.

FRET-FLIM detection and analysis

Hek293T cells were transfected with 1µg of pcDNA-*kcnk5b*-GFP and 1µg of the pcDNA6-Kirin-FRET sensor (Shen et al., 2019). Fluorescence lifetime imaging measurements were made by photon counting the fluorescence emission of CFP using a 2-photon-confocal Hyperscope (Scientifica, UK) and PMT-hybrid 40 MOD 5 photon detectors (Picoquant, Germany). Counted photon emissions were calculated and analyzed using SymPhoTime 64, version 2.4 (Picoquant, Germany).

Electrophysiology

Transfected HEK293T cells were seeded on glass coverslips (Fisher Brand), and incubated in cell culture medium at 37ºC, 5% CO_2, 95% relative humidity for 4-6 hours. The seeded coverslips were transferred into Tyrode's solution (138 mM NaCl, 4 mM KCl, 2 mM $CaCl_2$,1 mM $MgCl_2$, 0.33 mM NaH_2PO_4, 10 mM Glucose, 10 mM HEPES). Cells were assessed in the ruptured-patch whole-cell configuration of the patch-clamp technique using and EPC9 or EPC10 amplifier (HEKA) with borosilicate glass pipettes (Sutter Instruments) with 3-6 MΩ resistance when filled with pipette solution (130 mM glutamic acid, 10 mM KCl, 4 mM MgCl2, 10 mM HEPES, 2 mM ATP, pH to 7.2). After gigaseal formation, cells were voltage-clamped at -80 mV. Potassium conductance was elicited by test pulses from -100 mV to 70 mV (in 10mV increments) of 600 ms duration at a cycle length of 10s. The resulting tracings were converted into itx files by the ABF Software (ABF Software, Inc.) and then analyzed

using Clampfit™ Software (Molecular Devices). Currents were measured at the end of the test pulses.

Table 1 qRT-PCR primer sequences for zebrafish genes

F-lef1	AATGATCCCGTTCAAAGACG
R-lef1	CGCTAAGTCTCCCTCCTCCT
F-shha	CCACTACGAGGGAAGAGCTG
R-shha	GAGCAATGAATGTGGGCTTT
F-aldh1a2	AACCACTGAACACGGACCTC
R-aldh1a2	CTCCAGTTTGGCTCCTTCAG
F-pea3	AGAAGAACCGTCCAGCCATGA
R-pea3	AACATAACGCTCACCAGCCAC
F-msxb	ACACTTTGTCGAGCGTTTCGG
R-msxb	TCTTGTGCTTGCGTAAGGTGC
F-βactin	GCAGAAGGAGATCACATCCCTGGC
R-βactin	CATTGCCGTCACCTTCACCGTTC
F-Kcnk5b	ATCACTCTCCTCGTCTGCAACG
R-Kcnk5b	GAGTCCCATGCACAACGTGCAG
F-GFP	AAGGGCATCGACTTCAAGG
R-GFP	TGCTTGTCGGCCATGATATAG

Table 2 qRT-PCR primers for human genes

F-lef1	CTACCCATCCTCACTGTCAGTC
R-lef1	GGATGTTCCTGTTTGACCTGAGG
F-shh	CCGAGCGATTTAAGGAACTCACC
R-shh	AGCGTTCAACTTGTCCTTACACC
F-aldh1α2	GAGTAACTCTGGAACTTGGAGGC
R-aldh1α2	ATGGACTCCTCCACGAAGATGC
F-pea3	AGGAACAGACGGACTTCGCCTA
R-pea3	CTGGGAATGGTCGCAGAGGTTT
F-msx1	GACTCCTCAAGCTGCCAGAAGA
R-msx1	ACGGTTCGTCTTGTGTTTGCGG
F-GAPDH	GTCTCCTCTGACTTCAACAGCG
R-GAPDH	ACCACCCTGTTGCTGTAGCCAA

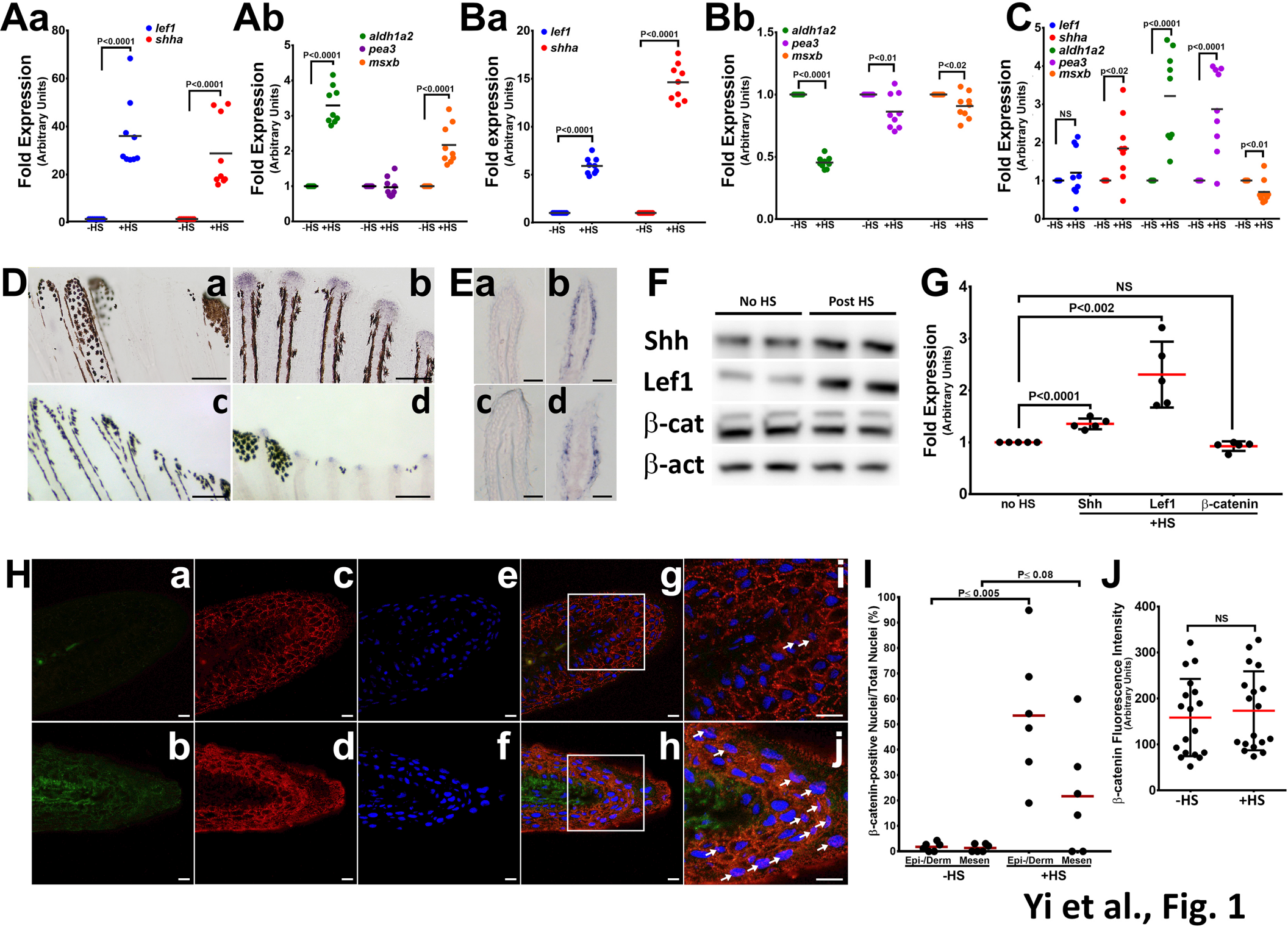
Aa
Fold Expression
(Arbitrary Units)
lef1
shha
P<0.0001
P<0.0001
-HS +HS -HS +HS
Ab
Fold Expression
(Arbitrary Units)
aldh1a2
pea3
msxb
P<0.0001
P<0.0001
-HS +HS -HS +HS -HS +HS
Ba
Fold expression
(Arbitrary Units)
lef1
shha
P<0.0001
P<0.0001
-HS +HS -HS +HS
Bb
Fold Expression
(Arbitrary Units)
aldh1a2
pea3
msxb
P<0.0001
P<0.01
P<0.02
-HS +HS -HS +HS -HS +HS
C
Fold Expression
(Arbitrary Units)
lef1
shha
aldh1a2
pea3
msxb
NS
P<0.02
P<0.0001
P<0.0001
P<0.01
-HS +HS -HS +HS -HS +HS -HS +HS -HS +HS
D
a
b
c
d
Ea
b
c
d
F
No HS
Post HS
Shh
Lef1
β-cat
β-act
G
Fold Expression
(Arbitrary Units)
NS
P<0.002
P<0.0001
no HS
Shh
Lef1
β-catenin
+HS
H
a
c
e
g
i
b
d
f
h
j
I
β-catenin-positive Nuclei/Total Nuclei (%)
P≤ 0.08
P≤ 0.005
Epi-/Derm
Mesen
Epi-/Derm
Mesen
-HS
+HS
J
β-catenin Fluorescence Intensity
(Arbitrary Units)
NS
-HS
+HS

Yi et al., Fig. 1

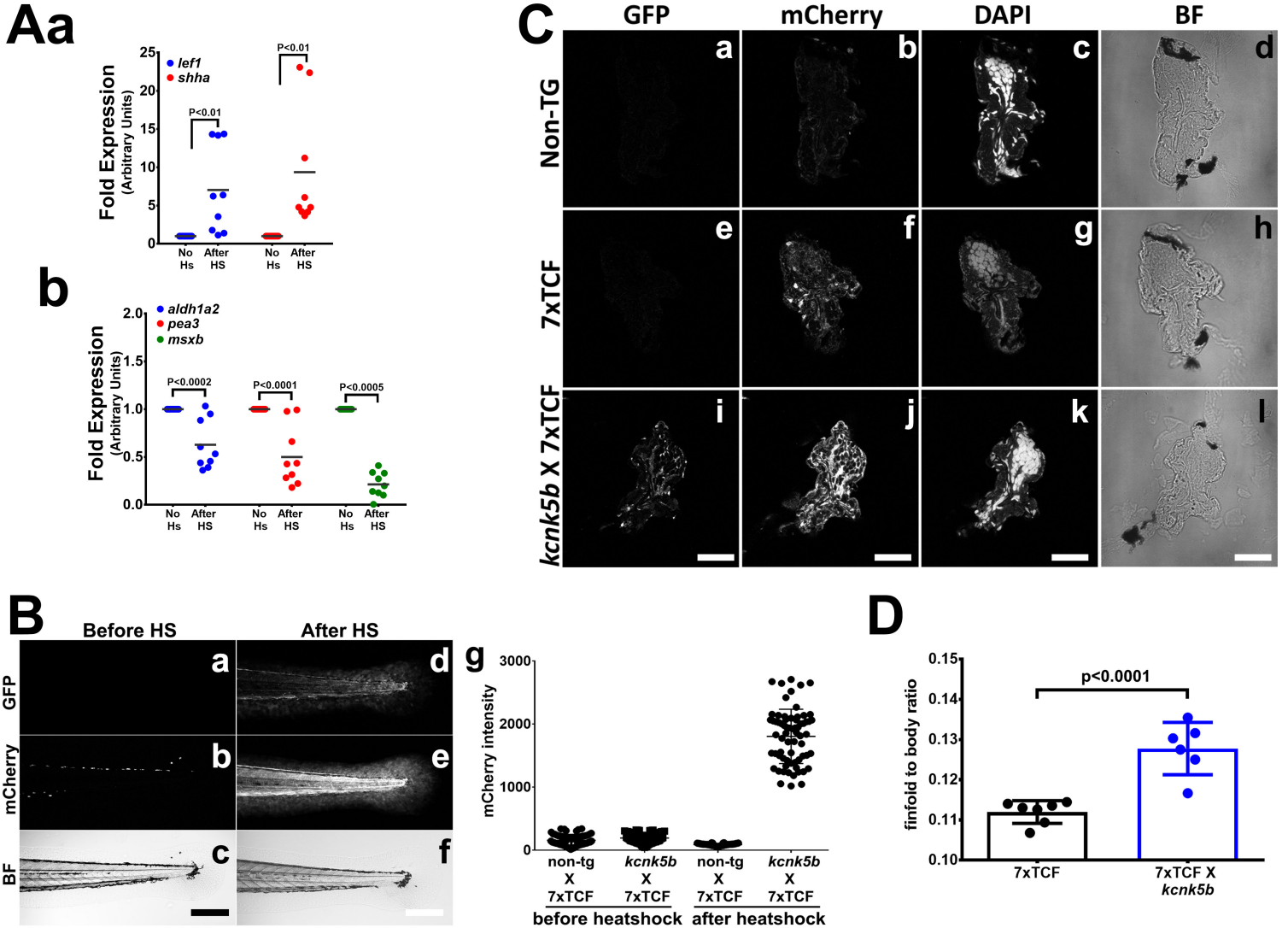
Aa
Fold Expression
(Arbitrary Units)
lef1
shha
P<0.01
P<0.01
No Hs
After HS
No Hs
After HS
b
Fold Expression
(Arbitrary Units)
aldh1a2
pea3
msxb
P<0.0002
P<0.0001
P<0.0005
No Hs
After HS
C
GFP
mCherry
DAPI
BF
Non-TG
7xTCF
kcnk5b X 7xTCF
B
Before HS
After HS
GFP
mCherry
BF
g
mCherry intensity
non-tg X 7xTCF
kcnk5b X 7xTCF
non-tg X 7xTCF
kcnk5b X 7xTCF
before heatshock
after heatshock
D
finfold to body ratio
p<0.0001
7xTCF
7xTCF X kcnk5b

Yi et al., Fig. 2

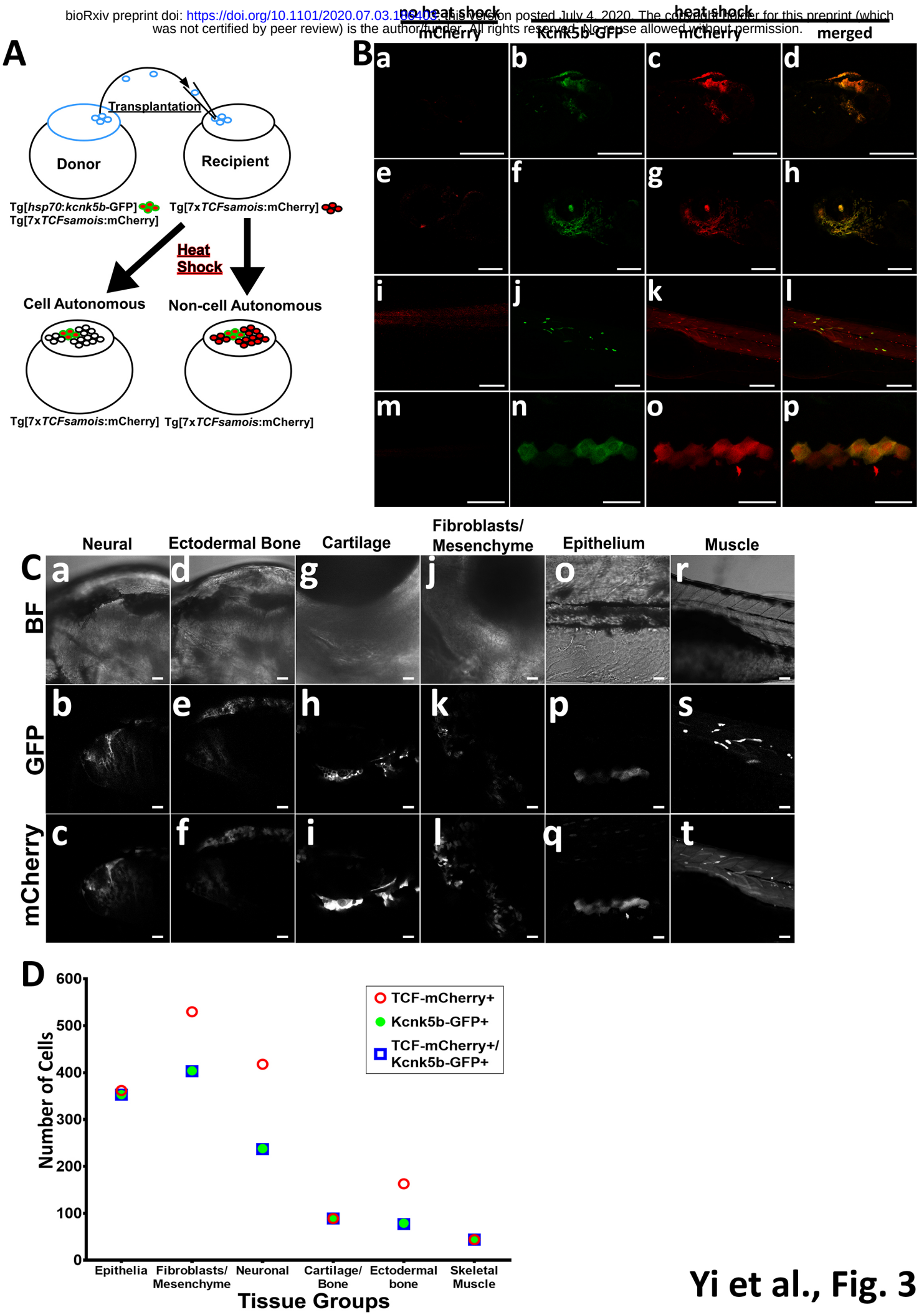

Yi et al., Fig. 3

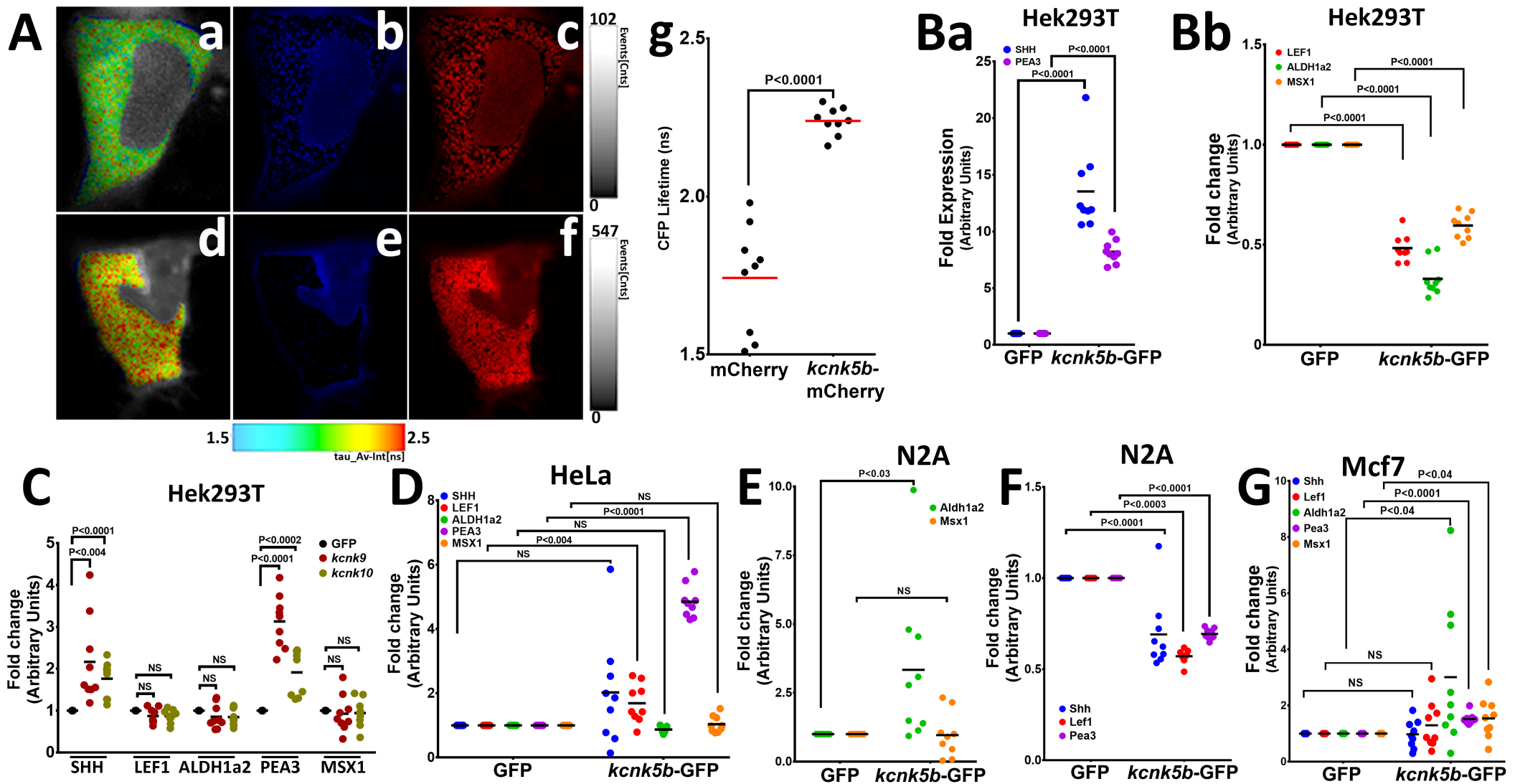

Yi el al., Figure 4

Yi et al., Figure 5

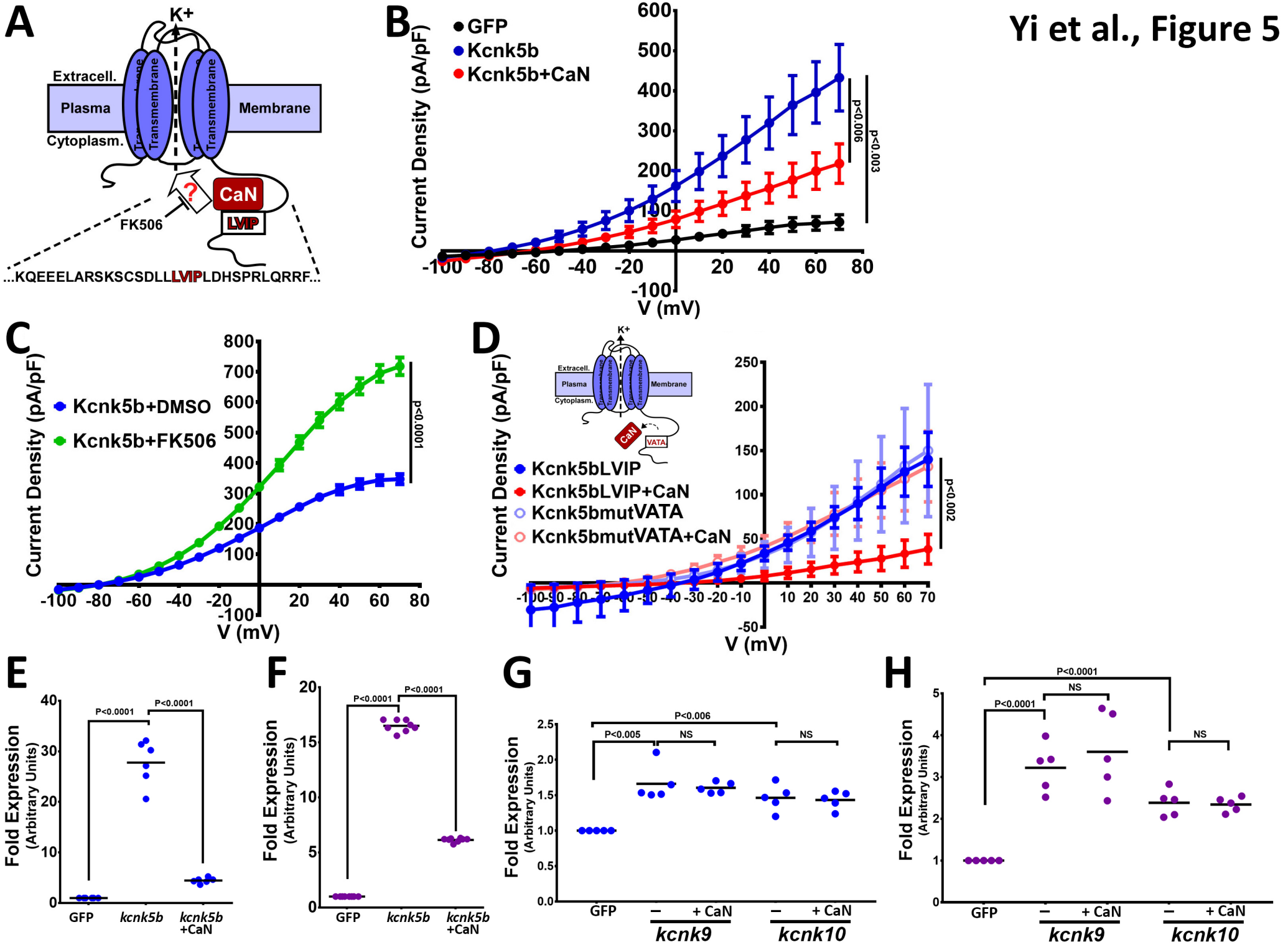

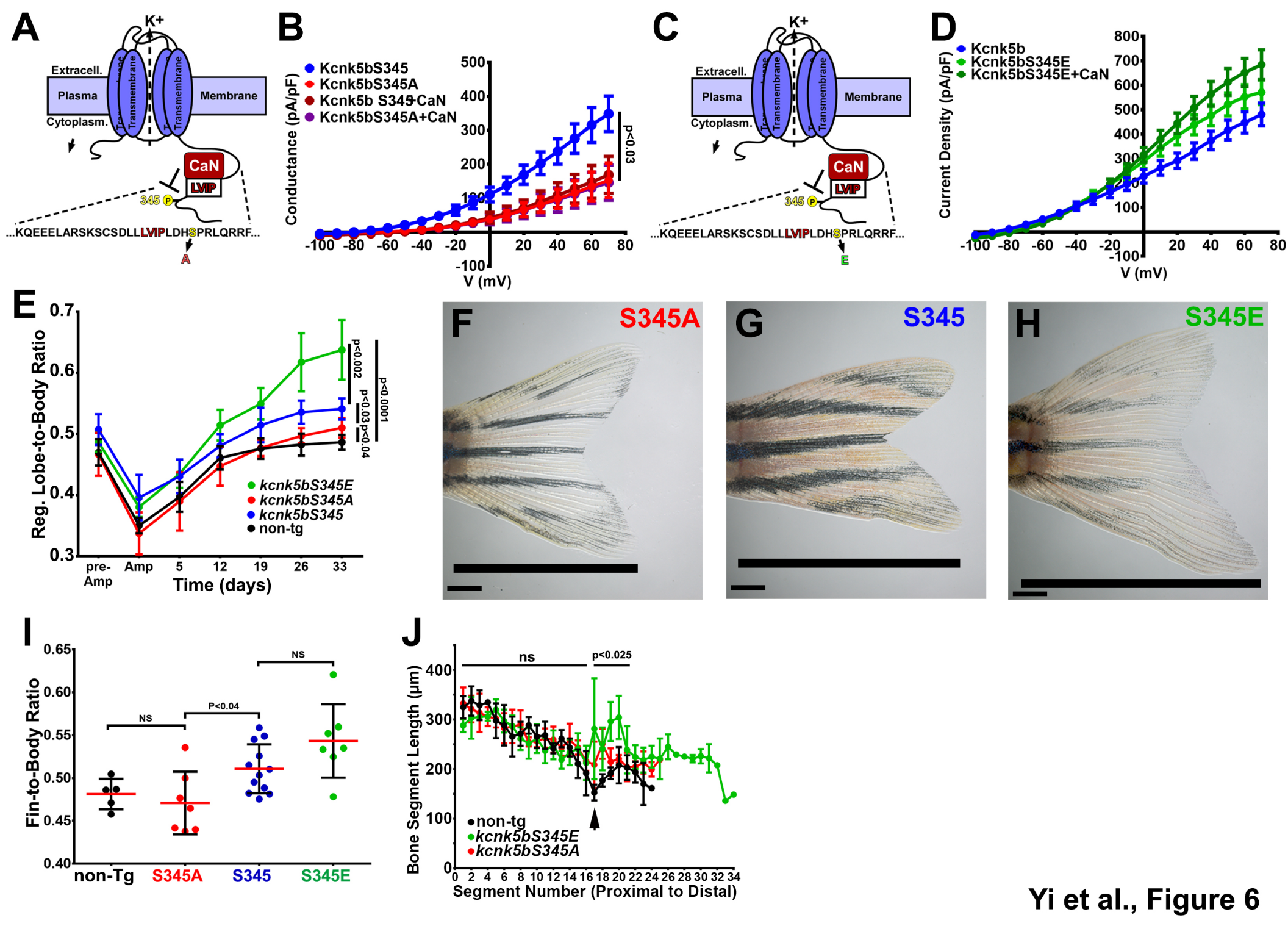

Yi et al., Figure 6

Yi et al., Figure 7

Scaling Information